Applied Energy 411 (2026) 127609



Contents lists available at ScienceDirect

Applied Energy

journal homepage: www.elsevier.com/locate/apenergy

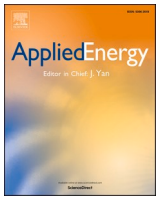

Toward improved siting of wind–solar hybrid farms: A novel framework integrating multi-criteria decision making, machine learning–driven feature selection, and spatial clustering

Yasin Ferit Uguz [1], Atakan Bilgili [*,1], Melis Uzar

Department of Geomatic Engineering, Yildiz Technical University, Istanbul 34220, Türkiye

HIGHLIGHTS

- Geographic decision framework screens sites for hybrid wind-solar power farms.
- Data-driven screening reduces 15 criteria to 9 key factors for clearer decisions.
- Suitability maps are grouped into practical site polygons for planning use.
- Multiple scoring and ranking runs identify sites that are robust across methods.
- Results align with existing wind turbines and solar plants in the study region.

ARTICLE INFO

Keywords:
Hybrid energy site selection
Geographic information systems
Multi-criteria decision making
Machine learning
Feature selection
Clustering

ABSTRACT

Ensuring secure, affordable, and sustainable energy supply is a growing global challenge as rising demand and supply insecurity accelerate the transition to renewable energy. Hybrid wind–solar systems offer an effective solution by exploiting spatial and temporal resource complementarity, but their deployment critically depends on reliable site selection. Most multi-criteria decision analysis studies rely on a single weighting method, apply limited criteria evaluation, lack statistical validation, and rarely identify spatially coherent, investment-ready zones. This study addresses these gaps by proposing an integrated geographic decision-making framework for hybrid wind–solar siting that combines two expert-based weighting methods, Analytical Hierarchy Process (AHP) and Best-Worst Method (BWM) with an objective, data-driven weighting method, CRiteria Importance Through Intercriteria Correlation (CRITIC) and machine learning–assisted criterion screening. The framework was applied to Izmir Province, Türkiye. Suitability maps generated under alternative weighting methods were compared using spatially adjusted statistical tests, clustered into contiguous high-suitability zones using hierarchical density-based spatial clustering (HDBSCAN), converted into candidate-site polygons, and prioritized using the Technique for Order Preference by Similarity to Ideal Solution (TOPSIS) and the Multi-Attributive Border Approximation Area Comparison (MABAC) method. The results revealed pronounced differences across weighting methods. Highly or very highly suitable areas accounted for 33.27% (AHP) and 27.75% (BWM) of candidate sites, compared with 58.39% under CRITIC. Validation using 703 existing solar photovoltaic and wind turbine installations showed agreement rates of 77.81%, 72.83%, and 83.65%, respectively. The resulting outputs provide actionable decision-support information for regional planning and the identification of investment-ready hybrid wind–solar zones.

* Corresponding author at: Davutpasa Street. Yildiz Technical University Davutpasa Campus, Faculty of Civil Engineering, Department of Geomatic Engineering, AZ-071, Türkiye.

E-mail address: atakanb@yildiz.edu.tr (A. Bilgili).

[1] The first two authors contributed equally to this work. For the purpose of academic records and professional advancement, both authors reserve the right to be listed as the first author in their respective Curriculum Vitae and grant applications.

https://doi.org/10.1016/j.apenergy.2026.127609
Received 18 September 2025; Received in revised form 26 January 2026; Accepted 22 February 2026
0306-2619/© 2026 Elsevier Ltd. All rights are reserved, including those for text and data mining, AI training, and similar technologies.

Abbreviations

AHP	Analytical Hierarchy Process
BWM	Best–Worst Method
CRITIC	CRiteria Importance Through Intercriteria Correlation
MCDM	Multi-Criteria Decision-Making
GIS	Geographic Information System
GIS–MCDM	GIS-based Multi-Criteria Decision-Making
ML	Machine Learning
MIG	Mutual Information Gain
SBFS	Sequential Backward Feature Selection
HDBSCAN	Hierarchical Density-Based Spatial Clustering of Applications with Noise
DBSCAN	Density-Based Spatial Clustering of Applications with Noise
MABAC	Multi-Attributive Border Approximation Area Comparison
TOPSIS	Technique for Order Preference by Similarity to Ideal Solution
SSM	Site Suitability Map
SPV	Solar Photovoltaic
PV	Photovoltaic
WT	Wind Turbine
LULC	Land Use/Land Cover
DEM	Digital Elevation Model
GHI	Global Horizontal Irradiance
SDG	Sustainable Development Goal
EU	European Union
UN	United Nations

Latin symbols

$\boldsymbol{A}$	Pairwise comparison matrix of criteria in AHP
$\boldsymbol{a_{ij}}$	Element of A; relative importance of criterion i over criterion j
$\boldsymbol{A^{norm}}$	Normalized pairwise comparison matrix in AHP
$\boldsymbol{a_{ij}^{norm}}$	Normalized element of the AHP comparison matrix in row i and column j
$\boldsymbol{w_{1,\ldots,n}}$	Weight vector of the criteria
$\boldsymbol{w_i}$	Weight of the *i-th* criterion
$\boldsymbol{B}$	Best (most important) criterion in BWM
$\boldsymbol{W}$	Worst (least important) criterion in BWM
$\boldsymbol{a_{Bj}}$	Preference of best criterion B over criterion j in BWM
$\boldsymbol{a_{jW}}$	Preference of criterion j over worst criterion W in BWM
$\boldsymbol{a_{BW}}$	Preference of best criterion B over worst criterion W
$\boldsymbol{w_B}$	Weight of the best criterion in BWM
$\boldsymbol{w_W}$	Weight of the worst criterion in BWM
$\boldsymbol{w_j^*}$	Optimal weight of criterion j obtained from the BWM model
$\boldsymbol{x_{ij}}$	Raw value of criterion j for spatial alternative i
$\boldsymbol{x_{ij}}$'	Normalized value of $\boldsymbol{x_{ij}}$ in CRITIC
$\boldsymbol{r_{jk}}$	Pearson correlation coefficient between criteria j and k
$\boldsymbol{C_j}$	Composite information score of criterion j
$\boldsymbol{w_j}$	Objective weight of criterion j in CRITIC
$\boldsymbol{VIF_i}$	Variance Inflation Factor of criterion i
$\boldsymbol{TOL_i}$	Tolerance value of criterion i
$\boldsymbol{R_i^2}$	Coefficient of determination when regressing criterion i on the others
$\boldsymbol{x}$	Sample values of variable x used in correlation analysis
$\boldsymbol{y}$	Sample values of variable y used in correlation analysis
$\boldsymbol{\bar{x}}$	Sample mean of x
$\boldsymbol{\bar{y}}$	Sample mean of y
$\boldsymbol{r_{xy}}$	Pearson correlation coefficient between x and y
$\boldsymbol{IG(X;Y)}$	Mutual information gain between variable X and target Y
$\boldsymbol{H(Y)}$	Entropy of the target variable Y
$\boldsymbol{H(Y\|X)}$	Conditional entropy of Y given X
$\boldsymbol{F}$	Set of all candidate features
$\boldsymbol{S}$	A subset of features
$\boldsymbol{S^*}$	Selected optimal feature subset
$\boldsymbol{k}$	Number of features in the selected subset
$\boldsymbol{M(S)}$	Merit of feature subset S
$\boldsymbol{d_i}$	Paired difference between two suitability values at location i
$\boldsymbol{n}$	Number of spatial units
$\boldsymbol{\alpha}$	Upper-tail fraction used to define top-α% of suitability
$\boldsymbol{T_\alpha}$	Suitability threshold corresponding to the top-α% of the suitability distribution
$\boldsymbol{A_\alpha}$	Set of cells belonging to the top-α% most suitable locations under baseline weights
$\boldsymbol{B_{\alpha,j,\pm 10\%}}$	Set of cells in the top-α% under the perturbed scenario of criterion j
$\boldsymbol{J_{\alpha,j,\pm 10\%}}$	Jaccard similarity between A_α and $B_\alpha\{\alpha,j,\pm 10\%\}$
$\boldsymbol{z_i}$	Suitability value at location i
$\boldsymbol{\bar{z}}$	Mean suitability
$\boldsymbol{w_{ij}}$	Spatial weight between locations i and j
$\boldsymbol{\bar{D}}$	Mean of paired differences
$\boldsymbol{s_D^2}$	Variance of paired differences
$\boldsymbol{n^{eff}}$	Effective sample size corrected for spatial autocorrelation
$\boldsymbol{\rho_k}$	Spatial autocorrelation of the difference series at lag k
$\boldsymbol{t^*}$	Spatially adjusted t-statistic for paired comparison of suitability maps
$\boldsymbol{X}$	Decision matrix; performance of alternative i on criterion j
$\boldsymbol{R}$	Normalized decision matrix in TOPSIS
$\boldsymbol{r_{ij}}$	Normalized value of x_{ij}
$\boldsymbol{V}$	Weighted normalized decision matrix in TOPSIS
$\boldsymbol{v_{ij}}$	Weighted normalized value of alternative i under criterion j
$\boldsymbol{A^+}$	Positive ideal solution (PIS)
$\boldsymbol{A^-}$	Negative ideal solution (NIS)
$\boldsymbol{S_i^+}$	Distance of alternative i from the positive ideal solution
$\boldsymbol{S_i^-}$	Distance of alternative i from the negative ideal solution
$\boldsymbol{C_i^*}$	Closeness coefficient of alternative i to the positive ideal solution
$\boldsymbol{N}$	Normalized decision matrix in MABAC
$\boldsymbol{n_{ij}}$	Normalized value of criterion j for alternative i in MABAC
$\boldsymbol{N'}$	Weighted normalized decision matrix in MABAC
$\boldsymbol{n'_{ij}}$	Weighted normalized value of criterion j for alternative i in MABAC
$\boldsymbol{g_j}$	Border Approximation Area (BAA) value for criterion j
$\boldsymbol{q_{ij}}$	Deviation of alternative i from the border approximation area g_j for criterion j
$\boldsymbol{Q_i}$	Overall MABAC score of alternative i
$\boldsymbol{\lambda_{max}}$	Principal eigenvalue of the AHP pairwise comparison matrix
$\boldsymbol{CI}$	Consistency Index in AHP
$\boldsymbol{CR}$	Consistency Ratio in AHP
$\boldsymbol{RI}$	Random Consistency Index in AHP
$\boldsymbol{\rho}$	Spearman rank correlation coefficient
$\boldsymbol{\xi}$	Maximum deviation parameter in the BWM consistency assessment
$\boldsymbol{\alpha}$	Upper-tail fraction used to define top-α% suitability

Parameters

C1	Land Use/Land Cover
C2	Distance to Protected Zones
C3	Distance to Water Bodies
C4	Distance to Airports
C5	Distance to Fault Lines
C6	Distance to Settlements
C7	Distance to Main Roads
C8	Distance to Energy Transmission Lines
C9	Distance to Substations

C10	Global Horizontal Irradiance	C13	Slope
C11	Wind Speed	C14	Aspect
C12	Annual Temperature	C15	Elevation

1. Introduction

Recent growth in electricity demand and recurring supply-security concerns are accelerating the shift toward low-carbon generation. At the same time, the air-pollution and climate impacts of fossil fuels, together with policy commitments such as the Paris Agreement, are driving rapid expansion of renewables; wind and solar have become leading options as their costs continue to decline [1–9]. Hybrid wind–solar systems co-locate solar photovoltaic (SPV) and wind turbine (WT) generation to exploit resource complementarity and shared infrastructure, improving supply adequacy and reducing curtailment and storage needs. Selecting locations for hybrid systems is therefore a multi-objective problem in which planners seek high energy yield while minimizing environmental and social impacts, implementation costs, and conflicts with regulations and public acceptance [10,11].

Geographic information system (GIS)-based multi-criteria decision making (MCDM) is widely used to integrate heterogeneous spatial criteria into suitability maps for renewable-energy planning [12–14]. However, recent reviews note that many hybrid siting studies (i) rely on a single weighting method, (ii) adopt buffer thresholds with limited justification, (iii) rarely test robustness or spatial statistical significance of outputs, and (iv) often stop at pixel-level maps without delineating investment-ready zones [10,13,14]. Within GIS-MCDM, Analytical Hierarchy Process (AHP) and Best-Worst Method (BWM) [15] are frequently used for expert weighting, while Technique for Order Preference by Similarity to Ideal Solution (TOPSIS) is often used to rank alternatives; more recently, objective weighting approaches such as CRiteria Importance Through Intercriteria Correlation (CRITIC) have been proposed to reduce subjectivity. Despite their contributions, existing GIS-based hybrid siting studies commonly exhibit four limitations: (1) method dependence due to reliance on a single weighting or ranking technique; (2) limited criterion screening prior to weighting, which can amplify redundancy and subjectivity; (3) limited statistical validation under spatial dependence; and (4) pixel-level outputs that do not directly translate into contiguous, investment-ready candidate zones.

To address these gaps, this study proposes an integrated GIS–MCDM–machine learning (ML) framework that leverages multiple MCDM weighting methods, ML-based criterion screening, spatial clustering combined with computational geometry approaches, and MCDM-based ranking techniques.

Table 1 synthesizes representative GIS-based siting studies and highlights the limited use of multi-method weighting, ML-based criterion screening, spatially adjusted validation, and polygon-level candidate delineation, thereby motivating the integrated workflow proposed in this study.

Motivated by the limitations identified in the recent literature, this study proposes a comprehensive GIS–MCDM–ML framework that integrates AHP, BWM, and CRITIC weighting methods with sensitivity analysis, ML-based feature selection, spatially adjusted statistical validation, and multiple ranking approaches to identify and prioritize suitable sites for hybrid wind–solar farms under Turkish regulatory constraints.

The proposed integration directly addresses key limitations of GIS-MCDM-based site screening:

(i) the use of three complementary weighting methods (AHP, BWM, and CRITIC) quantifies method-induced uncertainty and contrasts expert-driven and data-driven weight structures; (ii) ML-based feature selection reduces redundancy and prevents double-counting of correlated factors; (iii) HDBSCAN (Hierarchical Density-Based Spatial Clustering of Applications with Noise) clustering, combined with the Concave Hull algorithm, converts pixel-wise suitability outputs into investment-ready site polygons, enabling site-level alternatives; (iv) the application of two ranking techniques (TOPSIS and MABAC) tests ranking-method dependence and identifies consensus priorities; and (v) spatially adjusted statistical testing ensures that inter-method differences are evaluated under spatial dependence rather than inflated by autocorrelation.

Together, these steps yield (a) defensible suitability maps, (b) a shortlist of high-confidence candidate sites, and (c) an uncertainty-aware interpretation for planners. Accordingly, this study makes three practical contributions:

- It delivers a consensus-based shortlist of high-confidence candidate sites, supported by cross-method agreement metrics.

Table 1
Comparative summary of recent GIS-based MCDM and ML studies for renewable energy site selection.

Reference	Country / Region	Energy type	MCDM method(s)	ML / feature selection	Spatial statistical tests
Chaibi et al. [16]	Morocco	Wind	SF-AHP (spherical fuzzy AHP) + WASPAS	XGBoost + MLR for validation (no explicit FS)	Comparative & sensitivity analyses only (no explicit spatial tests)
Şahin et al. [17]	Türkiye	Wind	GIS–AHP	–	–
Yildiz [18]	Türkiye	Wind	AHP	–	Sensitivity analysis
Yaman [19]	Türkiye	Wind	GIS–AHP	–	–
Bilgili et al. [20]	Türkiye	Wind	(ML-centric approach)	Information Gain + ML models	Cochran's Q & McNemar
Kocabaldır and Yücel [21]	Türkiye	Solar	GIS+ AHP	–	Sensitivity analysis
Zalhaf et al. [22]	Sudan	Wind	GIS + FAHP	–	–
Saraswat et al. [23]	India	Solar + Wind	GIS + FAHP	–	–
Tercan E. [12]	Türkiye	Wind	GIS + BWM	–	–
Cunden et al. [24]	Mauritius	Wind	AHP + WLC	–	–
Soydan [25]	Türkiye	Solar	GIS + AHP	–	–
Giamalakiand Tsoutsos [26]	Greece	Solar + Concentrated solar	GIS + AHP	–	Sensitivity analysis
Merrouni et al. [27]	Morocco	Solar	GIS + AHP	–	–
Ali et al. [28]	Thailand	Solar + Wind	GIS + AHP	–	–
Ayodele et al. [29]	Nigeria	Wind	GIS + Interval type-2 fuzzy AHP	–	–

- It upgrades pixel-wise suitability maps into investment-ready site polygons via spatial clustering, enabling site-level decision-making.
- It improves credibility and interpretability by combining spatially adjusted inference with ML-driven criterion reduction to avoid redundancy.

2. Study area

Geographically positioned at 38°25′ N latitude and 27°8′E longitude, Izmir Province is the third most populous city in Türkiye as of 2022 [30].

Izmir Province's wind energy potential is particularly notable. Measurements in the Alaçatı region indicate average wind speeds of 8.11 m/s at an altitude of 70 m [31]. Analyses further show that wind speeds frequently exceed 7.5 m/s at this height, substantially enhancing the potential for energy generation [32].

The city also possesses considerable solar energy potential. Across Türkiye, the average annual sunshine duration is about 2640 h and the average annual solar radiation is approximately 1311 kWh/m^2-year [33], and Izmir Province, located in the Aegean region, benefits from these favorable national conditions. In addition to several techno-economic assessments for concentrating solar power plants in Izmir Province that report levelized electricity costs around 135 USD/MWh and operating costs of about 37.5 USD/MWh [34], the province hosts a rapidly growing portfolio of grid-connected SPV plants. As of 2024, Izmir Province's installed SPV capacity is on the order of 400 MW—corresponding to roughly 3–4% of Türkiye's total solar capacity—with numerous utility-scale facilities (e.g., SPV plants in Kemalpaşa, Tire, and Menemen districts) demonstrating the practical viability of solar deployment in the region [35]. Considering both resources jointly, Izmir Province represents one of the most promising regions in Türkiye for hybrid wind–solar energy systems, where the complementary wind and solar can enhance overall system performance (Fig. 1).

3. Methodology

In this study, the selection of most suitable sites for hybrid renewable energy systems (SPVs and WTs) was addressed through a comprehensive framework that integrates MCDM and data-driven screening techniques. The proposed framework is structured into four main phases (Fig. 2):

(1) Criteria definition and pre-processing – compiling socio-environmental, economic, climatic, and topographic criteria that influence the siting of hybrid energy systems.

(2) Criteria Weighting – assigning importance values to the criteria using the AHP and BWM, complemented by CRITIC method, to compare data-driven benchmark with expert-based weights.

(3) Investigation of the criteria – examining interrelations among the criteria through multicollinearity testing and Pearson correlation, and applying feature selection methods such as Mutual Information Gain (MIG) and Sequential Backward Feature Selection (SBFS) to determine their contribution to site suitability assessment using a clearly defined target variable and evaluation metric.

(4) Site Suitability Assessments – producing site suitability maps (SSMs), analyzing suitability score distributions, testing spatial dependence and method differences with spatially adjusted statistics, clustering suitable sites using HDBSCAN, and ranking the identified sites with the TOPSIS and MABAC methods.

3.1. Site selection criteria

Determining suitable locations for hybrid energy systems requires a site suitability analysis based on identifying criteria that significantly influence site selection. This involves defining assessment and restriction criteria that may enhance, reduce, or constrain the suitability of potential locations [12]. In this study, fifteen widely used site-selection criteria for wind and solar projects were identified through a comprehensive literature review and cross-checked against Turkish spatial planning principles, environmental regulations, and recent GIS-MCDM applications in Türkiye. These criteria were grouped into four dimensions—(i) socio-environmental, (ii) economic, (iii) climatic, and (iv) topographic—reflecting both international practice and national legislation. Table 2 presents the data sources and spatial resolution of each criterion, while Table 3 summarizes their frequency of adoption in



Fig. 1. Study area.

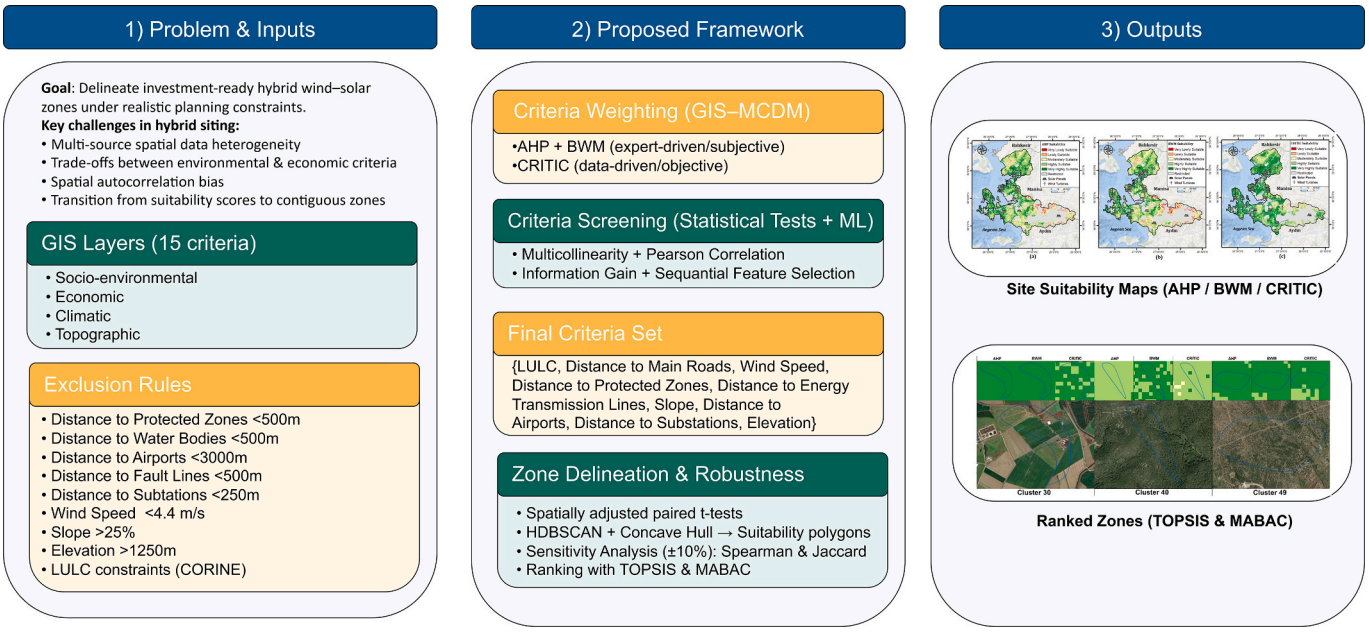

Fig. 2. Outline of the study.

Table 2
Sources of the site selection criteria.

ID	Category	Criterion	Format	Source
C1	Socio-Environmental	Land Use/Land Cover	Raster/ 100 m	CORINE Land Cover [36]
C2		Distance to Protected Zones	Vector	OpenStreetMap [37]
C3		Distance to Water Bodies	Raster/ 10 m	ESA Worldcover 2021 V200 [38]
C4		Distance to Airports	Vector	OpenStreetMap [37]
C5		Distance to Fault Lines	Vector	General Directorate of Mineral Research and Exploration of Türkiye [39]
C6		Distance to Settlements	Raster/ 10 m	ESA Worldcover 2021 V200 [38]
C7		Distance to Main Roads	Vector	OpenStreetMap [37]
C8	Economic	Distance to Energy Transmission Lines	Vector	OpenStreetMap [37]
C9		Distance to Substations	Vector	OpenStreetMap [37]
C10		Global Horizontal Irradiance	Raster/ 200 m	Global Solar Atlas [40]
C11	Climatic	Wind Speed	Raster/ 200 m	Global Wind Atlas [41]
C12		Annual Temperature	Raster/ 200 m	Global Solar Atlas [40]
C13		Slope	Raster/ 30 m	SRTM DEM [42]
C14	Topographic	Aspect	Raster/ 30 m	SRTM DEM [42]
C15		Elevation	Raster/ 30 m	SRTM DEM [42]

previous wind, solar, and hybrid siting studies. The widespread use of most selected criteria confirms their methodological relevance, while variability in adoption reflects differences in geographic context, regulatory frameworks, and data availability. Accordingly, the criteria used in this study were selected based on both their prevalence in the literature and their consistency with Turkish regulatory requirements, ensuring methodological robustness and regional relevance.

In hybrid energy siting, environmental, locational, and technical constraints must be explicitly considered to avoid unsuitable areas. These constraints are typically implemented through exclusion buffers around sensitive features (e.g., protected areas, water bodies, fault lines) and by removing incompatible land use/land cover (LULC) classes. Because no universal standards exist for buffer distances, thresholds are generally defined based on national regulations, regional planning principles, and expert judgments. In Türkiye, spatial constraints are guided by instruments such as the Environmental Impact Assessment Regulation, conservation principles, spatial development plans, and sector-specific guidelines. For example, recent national decisions specify minimum buffer distances of approximately 300 m from strictly protected areas and bird migration corridors [43], while watershed protection plans prohibit wind and solar installations within strictly protected drinking-water zones [44]. In addition, guidance from the Energy Market Regulatory Authority and the Turkish Civil Aviation Regulation requires wind turbines to be located at least 2 km from air–ground communication stations and 15 km from key navigation aids [45]. Where explicit Turkish regulations defined minimum distances (e.g., protected areas, airports, reservoirs), these values were adopted directly. Where regulations were absent (e.g., generic water bodies or fault lines), conservative thresholds were derived from recent GIS-MCDM siting studies conducted in Türkiye [12,19,46] and harmonized with international practice. The resulting exclusion thresholds are summarized in Table 4.

3.1.1. *Socio-environmental criteria*

Socio-environmental criteria assess the suitability of areas for renewable energy installations—such as SPV panels and WTs—based on sustainability and safety considerations.

Land Use/Land Cover: LULC is a key criterion for renewable energy siting, ensuring that essential land uses (e.g., agriculture, forests, protected areas) are preserved while directing development toward low-ecological-value areas such as bare land or sparsely vegetated terrain. Land eligibility constraints reduce conflicts by excluding urban areas, protected habitats, and highly productive agricultural zones [51] (Fig. 3 (a)).

Distance to Protected Zones: Represents proximity to ecologically

Table 3
Literature review for the identified site selection criteria.

Reference	C1	C2	C3	C4	C5	C6	C7	C8	C9	C10	C11	C12	C13	C14	C15
Chaibi et al. [16]	✓	✓	✓	✓		✓	✓	✓			✓		✓		✓
Şahin et al. [17]	✓		✓		✓	✓	✓	✓	✓	✓	✓	✓	✓	✓	✓
Yildiz [18]	✓				✓	✓	✓	✓	✓		✓		✓		
Yaman [19]	✓	✓	✓	✓	✓	✓	✓	✓	✓		✓		✓		✓
Bilgili et al. [20]		✓	✓	✓	✓	✓	✓	✓			✓		✓		✓
Kocabaldır and Yücel [21]			✓		✓	✓	✓	✓	✓	✓		✓	✓	✓	
Zalhaf et al. [22]	✓			✓		✓	✓	✓			✓		✓		✓
Saraswat et al. [23]	✓	✓	✓	✓		✓	✓	✓		✓	✓		✓	✓	✓
Tercan E. [12]	✓	✓	✓	✓	✓	✓	✓	✓			✓		✓		
Cunden et al. [24]		✓	✓	✓			✓	✓			✓		✓	✓	✓
Soydan [25]	✓		✓		✓	✓	✓	✓	✓	✓			✓	✓	
Giamalaki and Tsoutsos [26]	✓	✓	✓			✓	✓	✓		✓			✓	✓	✓
Ali et al. [28]	✓	✓		✓		✓	✓	✓		✓	✓		✓		✓
Ayodele et al. [29]	✓	✓	✓	✓		✓	✓	✓			✓		✓		✓

Table 4
Threshold values for the exclusion criteria.

Criterion	Exclusion value	Reference
LULC	Corine Code: 1.1.1,1.1.2,1.3.2,1.4.1,1.4.2,3.3.1,4.1.1,4.1.2, 4.2.1,4.2.2,4.2.3,5.1.1,5.1.2,5.2.1,5.2.2,5.2.3	Tercan [12]
Distance to Protected Zones	<500 m	Yaman [19]; Urfalı and Eymen [46]
Distance to Water Bodies	< 500 m	Yaman [19]; Urfalı and Eymen [46]; Noorollahi et al. [47]
Distance to Airports	< 3000 m	Yaman [19]; Zalhaf et al. [22]; Tercan [12]; Urfalı and Eymen [46]; Noorollahi et al. [47]; Gigovic et al. [48]
Distance to Fault Lines	< 500 m	Yildiz [18]; Moradi et al. [49]; Noorollahi et al. [50]
Distance to Substations	< 250 m	Yildiz [18]; Moradi et al. [49]
Wind Speed	< 4.4 m/s	Tercan [12]; Ayodele et al. [29]
Slope	> 25%	Tercan [12]; Latinopoulos and Kechagia [10]
Elevation	> 1250 m	Giamalaki and Tsoutsos [26]; Zalhaf et al. [22]

Note: The threshold values were selected to be consistent with Turkish environmental and spatial planning practice wherever possible, using national-scale GIS-MCDM studies and regional planning documents as primary references. International studies were only used where explicit Turkish regulations were not available, and conservative buffers were required.

and culturally sensitive areas, including national parks, nature reserves, cultural heritage sites, and archaeological zones [24]. Adequate separation is required to prevent ecological degradation, protect biodiversity, and preserve cultural landscapes, as associated infrastructure can fragment habitats and increase environmental pressures [52] (Fig. 3(b)).

Distance to Water Bodies: Indicates the distance to lakes, rivers, wetlands, and reservoirs. Renewable energy installations should avoid close proximity to water bodies to protect aquatic ecosystems and riparian habitats and to reduce construction complexity and costs [29] (Fig. 3(c)).

Distance to Airports: This criterion captures proximity to civil and military aviation facilities. WTs, in particular, can interfere with radar, navigation, and communication systems, posing risks to aviation safety; therefore, installations should maintain safe distances from airports [53] (Fig. 3(d)).

Distance to Fault Lines: Reflects the proximity to tectonically active zones. Maintaining adequate distance from fault lines reduces seismic risk, as SPVs/WTs and associated infrastructure near active faults may be vulnerable to structural damage during earthquakes [54] (Fig. 3(e)).

Distance to Settlements: Represents the distance to residential areas and built infrastructure. Adequate buffers help minimize visual impacts, reduce noise disturbance, and limit potential effects on public acceptance and property values[12,29] (Fig. 3(f)).

3.1.2. Economic criteria

Economic criteria assess site suitability for hybrid energy facilities based on accessibility and operational efficiency. These criteria aim to minimize logistical costs and optimize connections to existing infrastructure, such as roads, transmission lines, and substations. Proximity to utility networks facilitates site access, reduces the need for new infrastructure, and lowers both construction costs and associated environmental impacts [55]. In hybrid energy systems, such factors are critical for minimizing grid-connection costs, supporting construction logistics, and improving long-term operational reliability.

Distance to Main Roads: Represents the proximity to major transport infrastructure (e.g., highways, primary roads). Closer proximity improves site accessibility and reduces logistical costs, while excessive distance may increase infrastructure requirements and project costs. Adequate buffers are also needed to minimize visual disturbance, noise, and safety risks [22] (Fig. 4(a)).

Distance to Energy Transmission Lines: Refers to the proximity of existing grid infrastructure. Shorter distances reduce transmission losses and grid-connection costs and improve operational efficiency, although appropriate separation from sensitive receptors is required to ensure public safety and limit potential electromagnetic exposure [56,57] (Fig. 4(b)).

Distance to Substations: Reflects proximity to the electrical substations. Locations closer to substations facilitate grid integration, reduce transmission losses, and lower connection costs, thereby enhancing overall system efficiency (Fig. 4(c)).

3.1.3. Climatic criteria

Climatic criteria refer to atmospheric factors that directly influence the performance and long-term feasibility of SPVs and WTs. These variables are essential for estimating site energy potential, as solar output depends on radiation and temperature, while wind resources strongly

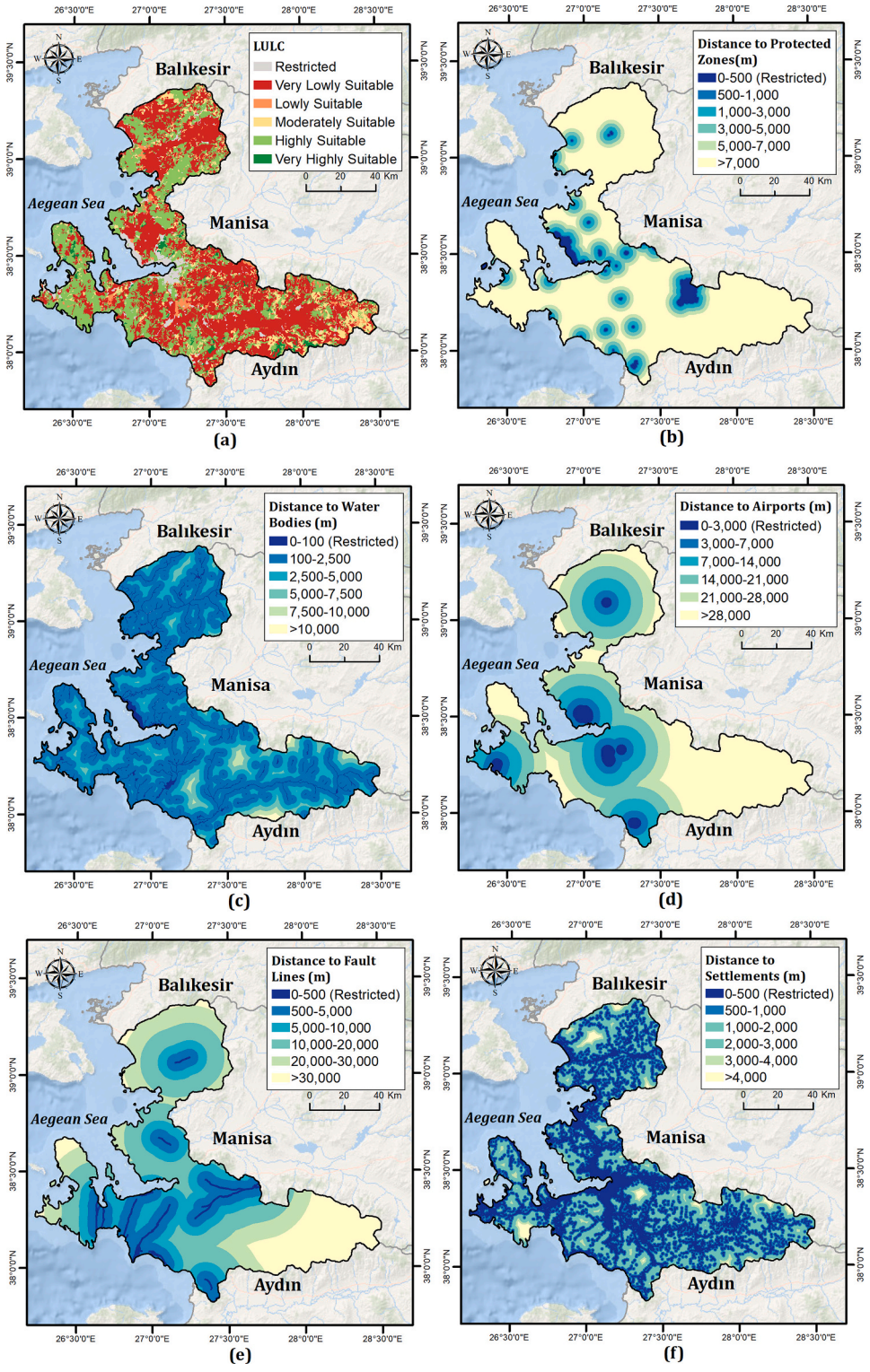

Fig. 3. Socio-environmental criteria maps.

affect turbine productivity. The complementary behavior of solar and wind resources further enhances system reliability, enabling hybrid systems to optimize energy yield and reduce supply variability [58].

Global Horizontal Irradiance (GHI): Represents the total solar radiation received per unit area on a horizontal surface and is a key parameter for estimating SPV energy output [59]. Izmir Province exhibits strong solar potential, with approximately 300 sunny days per year, up to 12 h of sunshine in summer, and annual radiation of 1500–1600 kWh/m^2, supporting high suitability for SPV deployment [60] (Fig. 5(a)).

Annual Average Wind Speed: Denotes the mean wind velocity at a location over one year and is the primary determinant of wind farm feasibility and productivity [12,22,49]. Izmir Province has substantial wind potential, with an estimated theoretical capacity of about 12,000 MW. The province currently accounts for ~20% of Türkiye's installed wind capacity, although only ~15% of its technical potential has been

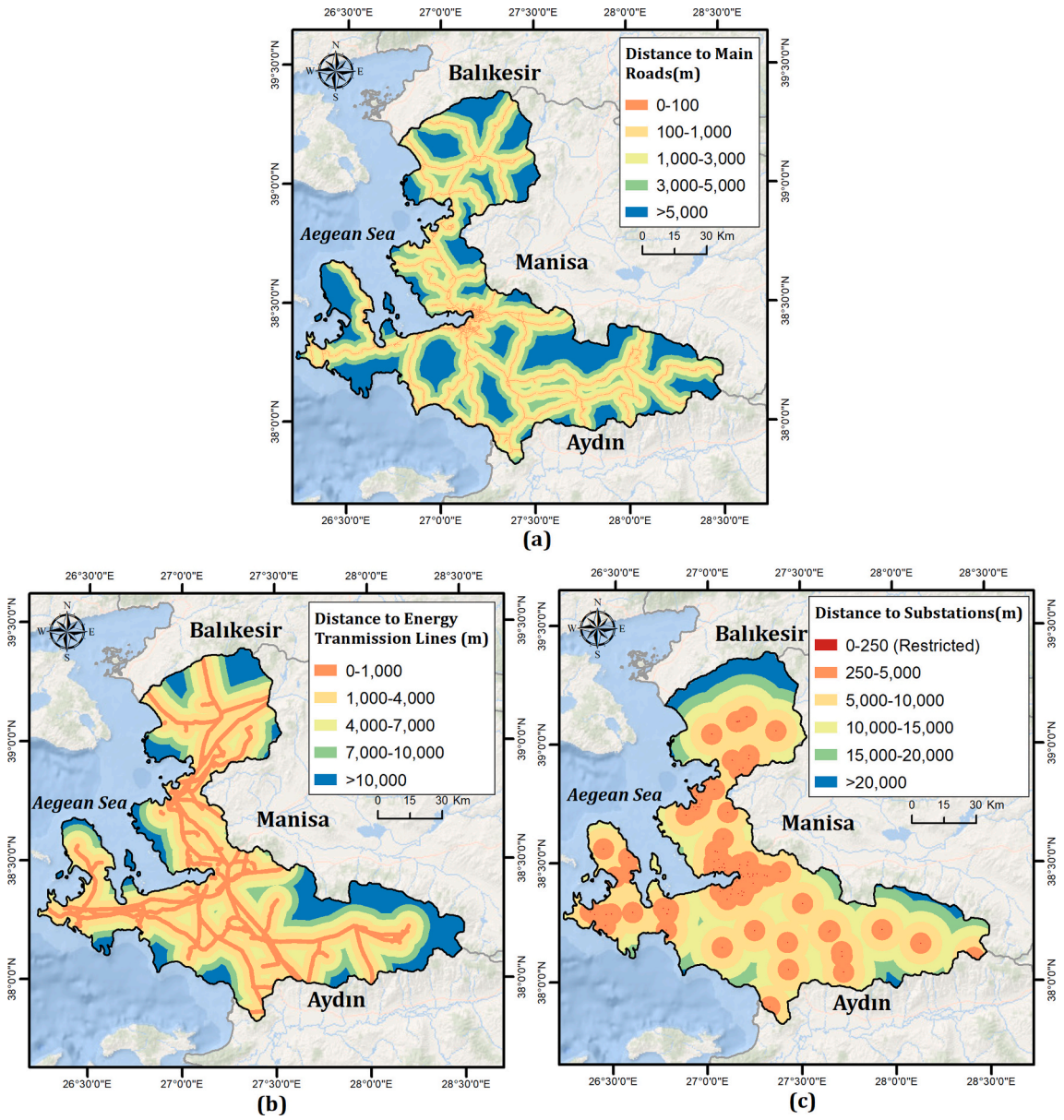

Fig. 4. Economic criteria maps.

utilized [61] (Fig. 5(b)). The hub height of the WTs considered in this study ranges from 75 to 105 m.

Annual Average Temperature: Reflects the long-term temperature conditions, which affect SPV performance. Higher temperatures reduce panel efficiency, with an estimated loss of ~0.45% per 1°C increase in panel temperature [21,62]. Therefore, sites with moderate temperatures are preferable for maximizing solar energy output (Fig. 5(c)).

3.1.4. Topographic criteria

Topographic criteria influence wind flow, solar exposure, construction feasibility, and land preparation requirements. Favorable topography improves resource efficiency while reducing project costs by facilitating site access, stable foundations, and minimizing environmental disturbance.

Slope: Reflects the terrain steepness and affects both energy performance and construction feasibility [23]. Low-slope areas are preferred, as steep terrain increases turbulence, distorts wind flow, and raises infrastructure and maintenance costs. Empirical evidence shows greater wind velocity deficits on steeper slopes, confirming their reduced suitability for wind energy development [47,63] (Fig. 6(a)).

Aspect: Denotes the orientation of terrain and directly influences solar exposure. In the Northern Hemisphere, south-facing and flat slopes receive higher annual solar radiation and are therefore more suitable for SPV installations, whereas north-facing slopes receive substantially less irradiation [23,64] (Fig. 6(b)).

Elevation: Represents the terrain height above sea level and influences both environmental sensitivity and project feasibility. High-elevation areas often present ecological constraints and limited infrastructure, increasing development complexity and costs, while lower elevations generally offer better accessibility and suitability for renewable energy installations [65] (Fig. 6(c)).

3.2. Weighting of the site selection criteria

MCDM methods are widely used to support complex decision problems, including renewable energy site selection [23]. Among these, the AHP proposed by Saaty [66] structures decision problems hierarchically and derives priorities through pairwise comparisons. However, AHP can

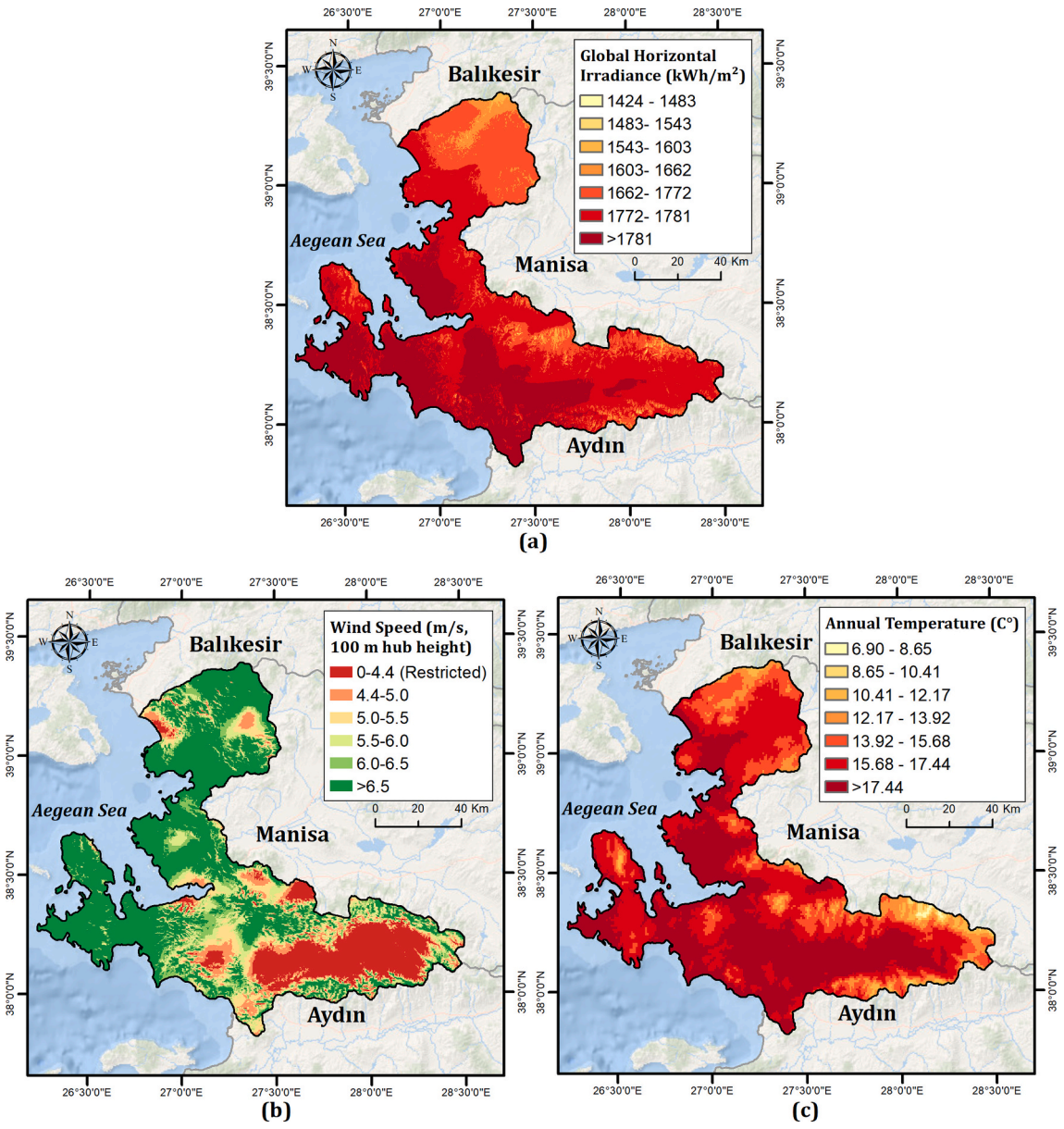

Fig. 5. Climatic criteria maps.

suffer from judgment inconsistency—especially as the number of criteria increases—high respondent burden due to numerous comparisons, eigenvector-related issues, and limited ability to represent interdependencies among criteria [66,67]. In particular, consistency often deteriorates when comparison matrices exceed 5 × 5. To address these limitations, Rezaei [15] proposed the BWM, which improves consistency while reducing cognitive burden. Unlike AHP, which require $\frac{n(n-1)}{2}$ comparisons for n criteria, BWM requires only $2n-3$ comparisons [15], making it more practical and reliable. Objective weighting approaches, such as CRITIC, have also gained attention as data-driven alternatives that reduce subjectivity.

Accordingly, this study integrates AHP, BWM, and CRITIC to capture complementary perspectives on criterion importance and to enhance methodological robustness. AHP represents comprehensive expert judgment, BWM provides a consistency-oriented expert approach, and CRITIC offers an objective, data-driven weighting mechanism. This design enables systematic comparison between expert-based and objective weighting strategies and evaluation of the stability of suitability patterns across fundamentally different weighting logics. Expert-based weights for AHP and BWM were elicited from five domain experts. To minimize individual bias, final criterion weights were obtained by averaging the weights across all experts. Expert profiles are summarized in Table 5.

3.2.1. AHP

The AHP is one of the most widely used MCDM methods for deriving criterion weights based on expert judgment [66]. In AHP, decision criteria are evaluated through pairwise comparisons using fundamental scale (Table 6), where experts express the relative importance of each criterion.

Based on expert evaluations, a pairwise comparison matrix $A = [a_{ij}]$ of size $n \times n$ is constructed (Eq. 1):

$$A = \begin{bmatrix} a_{11} & \cdots & a_{1j} & \cdots & a_{1n} \\ \vdots & & \vdots & & \vdots \\ a_{i1} & \cdots & a_{ij} & \cdots & a_{in} \\ \vdots & & \vdots & & \vdots \\ a_{n1} & \cdots & a_{nj} & \cdots & a_{nn} \end{bmatrix} \quad (1)$$

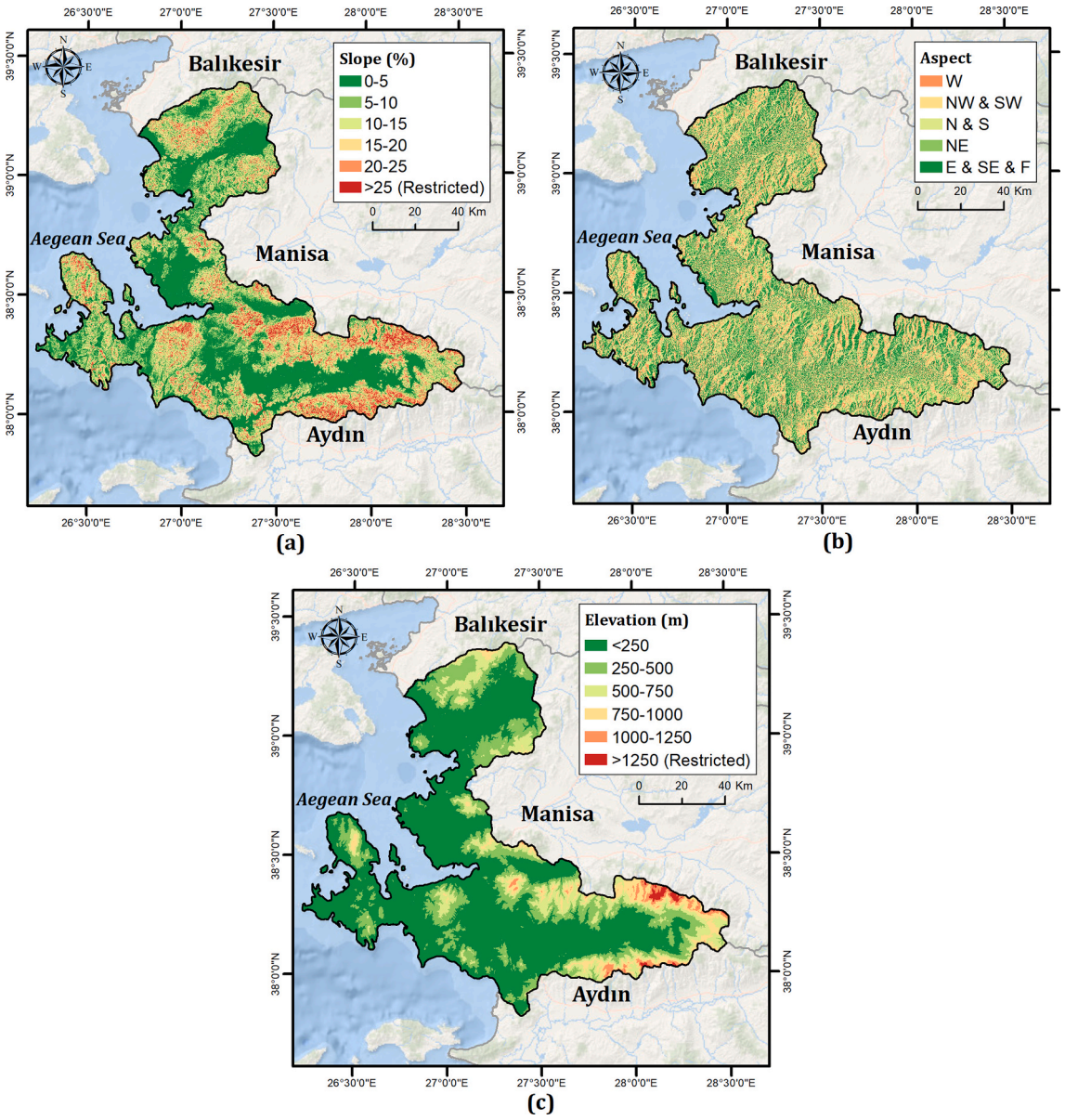

Fig. 6. Topographic criteria maps.

Table 5
Profile of the experts contributing to the AHP and BWM weighting process.

Expert ID	Field of Expertise	Current Role	Professional Experience
E1	Renewable Energy Planning	Energy systems analyst (public sector)	8 years
E2	GIS Specialist	Senior GIS specialist	10 years
E3	Environmental Engineering	Environmental impact analyst	7 years
E4	Electrical & Transmission Engineering	Power infrastructure engineer	12 years
E5	Urban & Regional Planning	Planning consultant	9 years

The matrix is normalized by dividing each element by the sum of its column (Eq. 2), and the weight of each criterion is obtained by averaging the normalized values across each row (Eq. 3):

Table 6
The pairwise comparison scale used for the criteria.

Description	Rank
Extreme Importance	9
Very Strong Importance	7
Strong Importance	5
Moderate Importance	3
Equal Importance	1
For compromise between the above values	2, 4, 6, and 8

$$a_{ij}^{norm} = \frac{a_{ij}}{\sum_{i=1}^{n} a_{ij}} \tag{2}$$

$$w_i = \frac{1}{n}\sum_{j=1}^{n} a_{ij}^{norm} \tag{3}$$

where w_i is the weight of the ith criterion, n is the total number of the criteria, a_{ij}^{norm} is the normalized element in row i, column j.

The consistency of expert judgments is evaluated using the Consis-

Table 7
Randomness index.

n	1	2	3	4	5	6	7	8	9	10	11	12	13	14	15
RI	0	0	0.58	0.90	1.12	1.24	1.32	1.41	1.45	1.49	1.51	1.48	1.56	1.57	1.59

tency Ratio (*CR*) (Eq. 5), which is calculated from the Consistency Index (*CI*) (Eq. 4) and the Random Index (RI) (Table 7):

$$CI = \frac{\lambda_{max} - n}{n - 1} \tag{4}$$

$$CR = \frac{CI}{RI} \tag{5}$$

where λ_{max} denotes the principal eigenvalue of matrix *A*. A *CR* value below 0.10 indicates acceptable consistency of expert judgments [66].

3.2.2. BWM

The BWM, proposed by Rezaei [15], is an efficient MCDM technique that requires fewer pairwise comparisons and generally yields higher consistency than traditional approaches such as AHP. For these reasons, it has been increasingly adopted in complex decision-making problems.

In BWM, the decision-maker first identifies the best (most important) criterion C_B and the worst (least important) criterion C_W. Two sets of pairwise comparisons are then provided using a scale from 1 to 9:

(i) the preference of the best criterion over all other criteria, forming the Best-to-Others vector A_B (Eq. 6), and (ii) the preference of all criteria over the worst criterion, forming the Others-to-Worst vector A_W (Eq. 7):

$$A_B = (a_{B1}, a_{B2}, a_{B3}, \ldots, a_{Bn}) \tag{6}$$

$$A_W = (a_{1w}, a_{2W}, a_{3W}, \ldots., a_{nW})^T \tag{7}$$

where α_{Bj}denotes the preference of the best criterion C_B over criterion *j*, and a_{jW} denotes the preference of criterion *j* over the worst criterion C_W.

The optimal criterion weights w_j^* are obtained by solving the following min–max optimization model (Eq. 8):

$$\min_{w,\xi} \xi \; subject\ to \left|\frac{w_B}{w_j} - a_{Bj}\right| \le \xi, \left|\frac{w_j}{w_w} - a_{jw}\right| \le \xi, \sum_{j=1}^{n} w_j = 1, w_j \ge 0 \; \forall_j \tag{8}$$

The consistency of expert judgments is evaluated using the BWM Consistency Ratio (*CR*) (Eq. 9), calculated as:

$$\mathrm{CR} = \frac{\xi}{\mathrm{CI}} \tag{9}$$

Where ξ is the optimal value obtained from Eq. (8), and *CI* is the maximum consistency index corresponding to the preference value a_{BW} (Table 8). Threshold values for acceptable consistency under different numbers of criteria are provided in Table 9. If the calculated *CR* is below the corresponding threshold, the judgments are considered sufficiently consistent; otherwise, the comparisons should be revised [15].

3.2.3. CRITIC

Objective, data-driven weighting approaches play an important role in reducing subjectivity and improving reproducibility in multi-criteria decision making. In this study, the CRITIC is employed as an objective weighting method [68]. CRITIC derives criterion importance from the intrinsic statistical structure of the dataset by considering two components: information content (variability) and discriminative power (independence). Criteria exhibiting higher variability and lower redundancy provide more useful information for distinguishing spatial alternatives.

Table 8
Maximum Consistency Index.

a_{BW}	1	2	3	4	5	6	7	8	9
Consistency Index (max ξ)	**0**	0.44	1	1.63	2.3	3	3.73	4.47	5.23

First, all criteria were normalized using a min–max transformation according to their preference direction (benefit or cost):

$$x'_{ij} = \frac{x_{ij} - \min(x_j)}{\max(x_j) - \min(x_j)} \; (benefit) \tag{10}$$

$$x'_{ij} = 1 - \frac{x_{ij} - \min(x_j)}{\max(x_j) - \min(x_j)} \; (cost) \tag{11}$$

The information content of each criterion is quantified using its variance:

$$y_j = \mathrm{var}\left(x'_j\right) \tag{12}$$

The discriminative power of each criterion is computed based on the mean absolute Pearson correlation with all other criteria:

$$d_j = 1 - \frac{1}{n-1} \sum_{k \ne j} |r_{jk}| \tag{13}$$

where r_{jk} is the Pearson correlation coefficient between criteria *j* and *k*. Higher d_j values indicate lower redundancy and greater independence.

These two components are combined to obtain a composite information score:

$$C_j = y_j \times d_j \tag{14}$$

Finally, objective criterion weights are obtained by normalizing the composite scores:

$$w_j = \frac{C_j}{\sum_{k=1}^{n} C_k}, \quad \sum_{j=1}^{n} w_j = 1, w_j \ge 0 \tag{15}$$

This fully objective weighting scheme provides a reproducible alternative to expert-based approaches such as AHP and BWM. In this study, the resulting CRITIC weights were compared with expert-based weights to evaluate robustness and methodological consistency.

3.3. Criteria investigation

Accurate identification of evaluation criteria is essential for reliable MCDM-based site selection. In this study, diagnostic and algorithmic feature-selection approaches were employed to enhance model robustness. Multicollinearity testing and Pearson correlation analysis were used as preliminary filters to remove redundant features. MIG assessed feature–target dependency, while SBFS identified the optimal subset of criteria. This multi-stage process ensured a statistically sound and informative feature set, supporting more reliable site suitability assessment.

3.3.1. Multicollinearity and Pearson correlation tests

Multicollinearity among criteria can reduce the reliability and interpretability of decision models. To diagnose this issue, Variance Inflation Factor (VIF) and Tolerance (TOL) were used. VIF was computed as:

Table 9
Thresholds for different numbers of criteria.

Criteria	3	4	5	6	7	8	9
3	0.2087	0.2087	0.2087	0.2087	0.2087	0.2087	0.2087
4	0.1581	0.2352	0.2738	0.2928	0.3102	0.3154	0.3283
5	0.2111	0.2848	0.3019	0.3309	0.3479	0.3611	0.3741
6	0.2164	0.2922	0.3565	0.3924	0.4041	0.4108	0.4298
7	0.209	0.3313	0.3734	0.3931	0.4035	0.4108	0.4299
8	0.2267	0.3409	0.4029	0.423	0.4379	0.4543	0.4599
9	0.2122	0.3653	0.4055	0.4225	0.4445	0.4587	0.4747

$$VIF_i = \frac{1}{1 - R_i^2} \tag{16}$$

where VIF_i denotes the variance inflation factor of the ith site selection criterion, and R_i^2 is the coefficient of determination obtained by regressing that criterion against all others. Following common practice, $VIF > 10$ *or* $TOL < 0.1$ was considered indicative of problematic multicollinearity.

When potential multicollinearity was detected, Pearson correlation analysis was applied to further examine pairwise relationships between criteria using:

$$r = \frac{\sum_{i=1}^{n}(x_i - \overline{x})(y_i - \overline{y})}{\sqrt{\sum_{i=1}^{n}(x_i - \overline{x})^2}\sqrt{\sum_{i=1}^{n}(y_i - \overline{y})^2}} \tag{17}$$

Criterion pairs with $|r| > 0.7$ were considered highly correlated, and one of the two variables was excluded to avoid redundancy. This procedure ensured that the final criterion set was statistically distinct and suitable for subsequent analyses.

3.3.2. MIG

MIG is a filter-based feature evaluation method that quantifies the dependency between an input criterion and the target variable. Higher MIG values indicate greater relevance for predicting the decision outcome. In this study, MIG was used to identify criteria that contribute most to site suitability in the MCDM framework.

MIG is defined as:

$$IG(X; Y) = H(Y) - H(YX) \tag{18}$$

where $IG(X; Y)$ denotes the mutual information between criterion X and target Y, $H(Y)$ is the entropy of the target variable, and $H(YX)$ is the conditional entropy of Y given X.

3.3.3. SBFS

SBFS is a wrapper-based feature selection method that iteratively removes the least informative criteria based on their impact on model performance. In this study, SBFS was applied in its backward form, starting with the full set of candidate criteria and progressively eliminating features that contributed least to the robustness of the decision framework. This procedure reduces redundancy and noise while retaining the most influential criteria for hybrid energy site selection.

The objective is to identify an optimal subset S^* of size k that maximizes a performance criterion:

$$S^* = \arg\max_{S \subseteq F, |S| = k} M(S) \tag{19}$$

where F denotes the full feature set, S is a candidate subset, k is the number of selected criteria, $M(S)$ represents the evaluation score of subset S.

3.4. Sensitivity analysis of MCDM methods

To evaluate the robustness of suitability maps derived from AHP, BWM, and CRITIC, a sensitivity analysis was conducted. Sensitivity analysis is a standard component of MCDM frameworks, assessing how variations in criterion weights affect model outputs and spatial decision patterns [69]. In spatial applications, robustness must be evaluated not only in terms of ranking stability but also in terms of spatial persistence of highly suitable areas.

Accordingly, two complementary indicators were employed:

(i) Spearman rank correlation, to assess stability of suitability rankings, and

(ii) Jaccard similarity, to evaluate the spatial consistency of high-suitability zones.

3.4.1. Weight perturbation

For each weighting method (AHP, BWM, and CRITIC), baseline suitability scores were first computed. Sensitivity to weight uncertainty was then assessed by applying a controlled ±10% perturbation to each criterion weight, consistent with established MCDM robustness analyses [70,71]. After perturbation, remaining weights were proportionally rescaled to satisfy the unit-sum constraint. This procedure generated multiple perturbed scenarios for systematic comparison with baseline results.

3.4.2. Ranking stability

Ranking robustness was quantified using the Spearman rank correlation coefficient between baseline suitability scores S and perturbed scores $S^{(j,\pm 10\%)}$:

$$\rho_{S,S(j,\pm 10\%)} = 1 - \frac{6\sum_{i=1}^{m} d_i^2}{m(m^2 - 1)} \tag{20}$$

where d_i denotes the rank difference of cell i between baseline and perturbed scenarios. Values close to 1 indicate high ranking stability and strong robustness.

3.4.3. Spatial consistency of high-suitability areas

Spatial robustness was evaluated by examining the persistence of high-suitability areas. The top 5%, 10%, and 20% quantiles of suitability scores were extracted for both baseline and perturbed scenarios [72]. The threshold for the top α fraction is defined as:

$$T_\alpha = Q_{1-\alpha}(S) \tag{21}$$

The corresponding high-suitability sets are:

$$A_\alpha = \{i : S_i \geq T_\alpha\}, B_\alpha^{(j,\pm 10\%)} = \left\{i : S_i^{(j,\pm 10\%)} \geq T_\alpha^{(j,\pm 10\%)}\right\} \tag{22}$$

Spatial agreement between baseline and perturbed sets was quantified using the Jaccard similarity index:

$$J_\alpha^{(j,\pm 10\%)} = \frac{\left|A_\alpha \cap B_\alpha^{(j,\pm 10\%)}\right|}{\left|A_\alpha \cup B_\alpha^{(j,\pm 10\%)}\right|} \tag{23}$$

Values approaching 1 indicate strong spatial stability of high-suitability zones.

The sensitivity analysis was applied consistently to AHP, BWM, and CRITIC to enable direct comparison of robustness across weighting strategies. By jointly evaluating ranking stability and spatial persistence, the framework provides a rigorous basis for assessing whether small perturbations in weights materially affect suitability patterns.

3.5. Site suitability assessments

Site suitability assessment was performed using a structured, multi-stage workflow. SSMs were first generated using AHP, BWM, and CRITIC within a weighted-sum framework. High-suitability areas were then grouped into spatially coherent zones using the HDBSCAN clustering algorithm [73]. These clusters were converted into polygon-based candidate sites using the Concave Hull algorithm [74]. Finally, the resulting polygons were ranked using TOPSIS [75], and MABAC methods to prioritize the most suitable locations. This integrated procedure enables both spatial refinement and systematic prioritization of candidate hybrid energy sites.

3.5.1. Generation of the SSMs

SSMs were generated in a GIS environment using a weighted sum model that integrates criterion weights derived from MCDM methods with the corresponding raster layers:

$$\sum_{i=1}^{n} w_i \times r_i \tag{24}$$

where w_i denotes the weight and r_i the raster layer of the ith (criterion)

Pairwise comparisons were first performed for the initial set of 15 criteria and subsequently repeated for the refined subset identified through the feature selection process. The resulting suitability scores were classified into five suitability classes and analyzed across the study area. Differences between SSMs were evaluated using a spatially adjusted paired-samples *t*-test to assess statistical significance.

3.5.2. Statistical comparison of suitability values

SSMs produced by GIS-MCDM are spatially continuous surfaces; therefore, pixel values are not statistically independent. Ignoring spatial dependence can inflate significance levels and bias inference. For this reason, spatial autocorrelation was explicitly assessed prior to comparing suitability values derived from AHP, BWM, and CRITIC.

Global spatial dependence was evaluated using Global Moran's I:

$$I = \frac{n}{W} \cdot \frac{\sum_{i=1}^{n}\sum_{j=1}^{n} w_{ij}(z_i - \bar{z})(z_j - \bar{z})}{\sum_{i=1}^{n}(z_i - \bar{z})^2} \tag{25}$$

where z_i is the suitability value at location $i, \bar{z}$ is the global mean, w_{ij} denotes the spatial weight between locations i and $j, W = \sum_i \sum_j w_{ij}$, and n is the total number of spatial units.

When significant spatial autocorrelation was detected, conventional paired *t*-tests were considered inappropriate. Accordingly, a spatially adjusted paired comparison was applied to compare AHP–BWM, AHP–CRITIC, and BWM–CRITICsuitability values. The adjusted test statistic is:

$$t^{*} = \frac{\bar{D}}{\sqrt{s_D^2 / n_{eff}}} \tag{26}$$

where $\bar{D}$ denotes the mean paired difference, s_D^2 is the variance of the differences, and n_{eff} is the effective sample size corrected for spatial autocorrelation:

$$n_{eff} = \frac{n}{1 + 2\sum_{k=1}^{K} \rho_k} \tag{27}$$

Here, ρ_k denotes spatial autocorrelation at lag k, estimated from the spatial correlogram, and K is the maximum lag considered.

3.5.3. Generation of the site suitability polygons

High-suitability locations (suitability $\geq$4) were clustered using the HDBSCAN algorithm [73] to identify spatially coherent candidate zones. HDBSCAN detects clusters across varying density levels, enabling robust identification of groups with different shapes and densities without requiring prior specification of the number of clusters. It also distinguishes meaningful clusters from low-density noise points, thereby improving the reliability of spatial delineation.

The resulting clusters were converted into site suitability polygons using the Concave Hull algorithm [76]. Unlike convex hulls, which tend to overgeneralize spatial boundaries, concave hulls preserve local geometric detail and produce more realistic polygon representations. This approach enabled the delineation of accurate, investment-ready candidate zones suitable for subsequent ranking and decision analysis.

3.6. Ranking of the site suitability polygons

After delineating the site suitability polygons, candidate locations were ranked to support investment prioritization. Criterion weights derived from BWM were combined with the polygons generated via HDBSCAN clustering and the Concave Hull algorithm and used as inputs to the ranking-based MCDM methods, TOPSIS and MABAC, to obtain the final rankings. To enhance robustness and reduce method-specific bias, both methods were applied and the consistency between their results was evaluated.

3.6.1. TOPSIS

TOPSIS ranks alternatives based on their distances to the positive ideal solution and the negative ideal solution [75].

Let $X = [x_{ij}]$ denote the decision matrix of size $m \times n$, where m is the number of alternatives (site polygons) and n is the number of criteria:

$$X = \begin{bmatrix} x_{11} & x_{12} & \cdots & x_{1n} \\ x_{21} & x_{22} & \cdots & x_{2n} \\ \vdots & \vdots & \ddots & \vdots \\ x_{m1} & x_{m2} & \cdots & x_{mn} \end{bmatrix} \tag{28}$$

The matrix is normalized using vector normalization:

$$r_{ij} = \frac{x_{ij}}{\sqrt{\sum_{i=1}^{m} x_{ij}^2}}, i = 1, 2, \ldots, m; j = 1, 2, \ldots, n \tag{29}$$

Criterion weights w_j are applied to obtain the weighted normalized matrix:

$$v_{ij} = w_j r_{ij} \tag{30}$$

The positive ideal solution A^+ and negative ideal solution A^- are defined as:

$$A^{+} = \left\{ \left(\max_i v_{ij} \middle| j \in J \right), \left(\min_i v_{ij} \middle| j \in J' \right) \right\} = \left\{ v_1^+, v_2^+, \ldots, v_n^+ \right\} \tag{31}$$

$$A^{-} = \left\{ \left(\min_i v_{ij} \middle| j \in J \right), \left(\max_i | v \in J' \right) \right\} = \left\{ v_i^-, v_2^-, \ldots, v_n^- \right\} \tag{32}$$

where J and J' represent benefit and cost criteria, respectively.

The separation distances of each alternative from the ideal solutions are calculated using Euclidean distance:

$$S_i^{+} = \sqrt{\sum_{j=1}^{n} \left(v_{ij} - v_j^{+} \right)^2} \tag{33}$$

$$S_i^{-} = \sqrt{\sum_{j=1}^{n} \left(v_{ij} - v_j^{-} \right)^2} \tag{34}$$

Finally, the relative closeness coefficient is computed as:

$$C_i^* = \frac{S_i}{S_i^+ + S_i^i} \tag{35}$$

Higher C_i^* values indicate more suitable alternatives.

3.6.2. MABAC

The MABAC method is a ranking-based MCDM approach that evaluates alternatives according to their distances from criterion-specific border approximation areas (BAA) [77]. Owing to its numerical stability and robustness, MABAC has been increasingly applied in spatial decision-making problems.

Let $X = [x_{ij}]$ denote the decision matrix of size $m \times n$, where m is the number of alternatives (site polygons) and n is the number of criteria:

$$X = [x_{ij}]_{m\times n} \tag{36}$$

The matrix is normalized using min–max normalization for benefit and cost criteria:

$$r_{ij} = \frac{x_{ij} - \min(x_j)}{\max(x_j) - \min(x_j)} \tag{37}$$

$$r_{ij} = \frac{\max(x_j) - x_{ij}}{\max(x_j) - \min(x_j)} \tag{38}$$

The weighted normalized matrix is computed as:

$$v_{ij} = w_j(r_{ij} + 1) \tag{39}$$

The border approximation area for each criterion is defined as the geometric mean of the weighted normalized values:

$$g_j = \left(\prod_{i=1}^{m} v_{ij}\right)^{1/m} \tag{40}$$

The deviation of each alternative from the border area is calculated as:

$$q_{ij} = v_{ij} - g_j \tag{41}$$

Final ranking scores are obtained by aggregating deviations across all criteria, with higher overall values indicating more suitable alternatives.

4. Results and discussion

4.1. Simulation environment

GIS-based spatial analyses and suitability map generation were conducted using ArcGIS Pro (v3.5). Data pre-processing, ML–based feature selection, statistical analyses, clustering (HDBSCAN), sensitivity analysis, and MCDM computations were implemented in Python (v3.8) using standard scientific libraries, including NumPy, Pandas, Scikit-learn, and related packages. All simulations and computations were executed on a Windows-based workstation equipped with an Intel® Core™ i7 processor and 32 GB of RAM.

4.2. Initial weighting and criteria investigation

Pairwise comparisons were performed on the initial fifteen criteria using AHP and BWM (Section 3.1). Based on these weights (Appendix A), preliminary SSMs were generated using a weighted sum model. The resulting dataset was then examined to refine the criteria set. Multicollinearity analysis (Table 10) revealed a maximum VIF of 17.737 and a minimum TOL of 0.056, indicating that two criteria—annual temperature and elevation—exceeded acceptable thresholds and required further evaluation.

Pearson correlation analysis (Fig. 7) confirmed strong correlations among three criterion pairs (C12–C15, C2–C5, and C2–C4), consistent with the multicollinearity results. Consequently, within the highly correlated C12–C15 pair, annual temperature was excluded due to its coarser spatial resolution relative to elevation (200 m vs. 30 m). Excluding annual temperature reduces redundancy and prevents double-counting of overlapping topography–climate information in subsequent weighting and suitability analyses.

Table 10
Results of the multicollinearity tests.

Site Selection Criteria	VIF	TOL
C1	4.329	0.231
C2	3.138	0.319
C3	1.456	0.687
C4	3.585	0.279
C5	3.407	0.294
C6	1.537	0.651
C7	1.525	0.656
C8	2.083	0.480
C9	1.744	0.573
C10	2.958	0.338
C11	1.523	0.656
C12	17.737	0.056
C13	1.485	0.673
C14	4.255	0.235
C15	13.034	0.077

The strong correlation between C12 and C15 is expected, as temperature generally decreases with increasing elevation. The correlation observed between C2 and C4 is also plausible, since airports and protected zones often occur in peripheral or undeveloped areas where large land parcels are reserved for safety buffers or conservation. A similar spatial logic explains the C2–C5 relationship, as protected areas are frequently designated in mountainous or geologically distinct regions where active faults are common and intensive development is restricted.

To further refine the criteria set, two algorithm-based feature selection methods were applied: MIG and SBFS. The MIG results (Fig. 8) identified C11, C13, and C7 as the most informative criteria; however, MIG primarily serves as a relevance check rather than a robust reduction tool. Therefore, SBFS was adopted as the main criterion-selection method, with MIG used as a complementary indicator. Based on SBFS implemented with a Random Forest model [78], nine criteria were retained as the final set: {C1, C2, C4, C7, C8, C9, C11, C13, C15}.

A notable outcome is the exclusion of GHI by SBFS, despite its frequent importance in SPV siting studies [31,32]. To assess whether this reflects methodological bias or a regional characteristic, solar-resource variability was compared between the full study area and the feasible area after exclusions (Appendix B, Table A1). GHI exhibits very low spatial variability in both domains (mean = 1750.96 vs. 1747.94 kWh/m^2/yr; CV = 2.672% vs. 2.722%), indicating that solar resource is uniformly high and offers limited discriminative power. By contrast, wind speed shows substantially higher variability (CV = 26.48% and 18.86%; Appendix B, Table A2), explaining its stronger contribution to site differentiation.

Considering these results, criterion investigation prior to weighting is essential in GIS-based MCDM. Reducing redundancy enhances model robustness and lowers expert cognitive burden, thereby supporting more reliable weighting and more interpretable suitability maps.

4.3. Final criteria weights

Following the criteria investigation, pairwise comparisons were repeated for both AHP and BWM until convergence on a stable criteria set was achieved. Main-criteria weights are reported in Appendix C, and sub-criteria weights derived from AHP and BWM are presented in Table 11.

Across experts, some variation in individual judgments was observed: Experts 1, 3, and 5 assigned equal importance to all four dimensions, Expert 2 emphasized Socio-Environmental and Economic

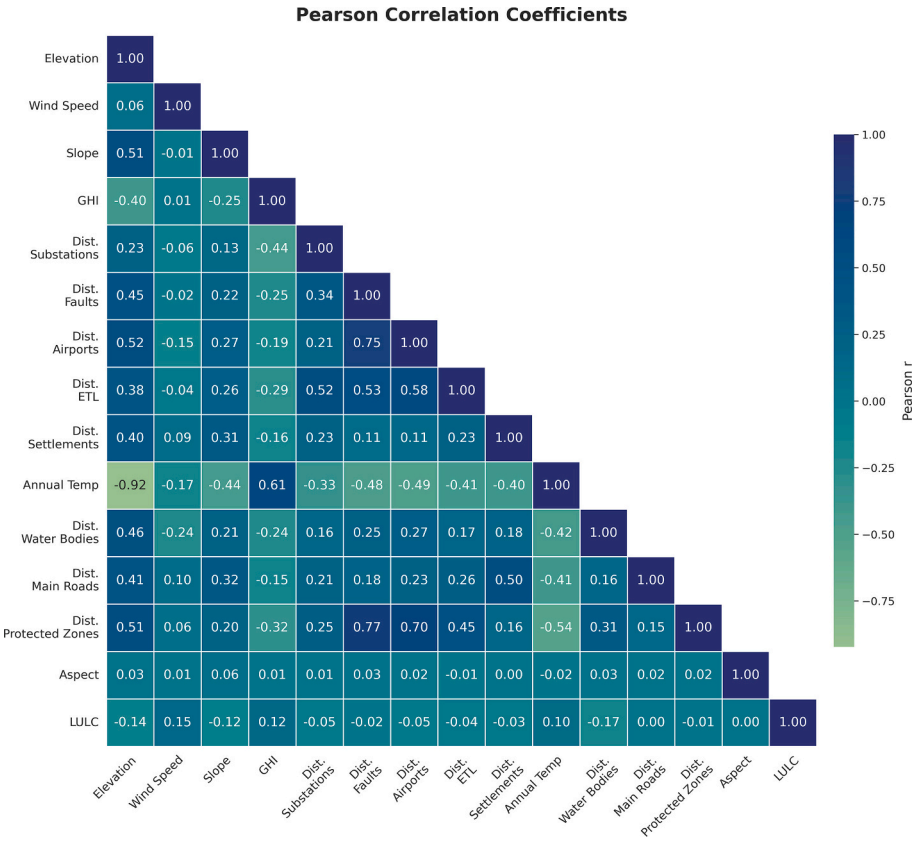

Fig. 7. Correlation matrix of the criteria.

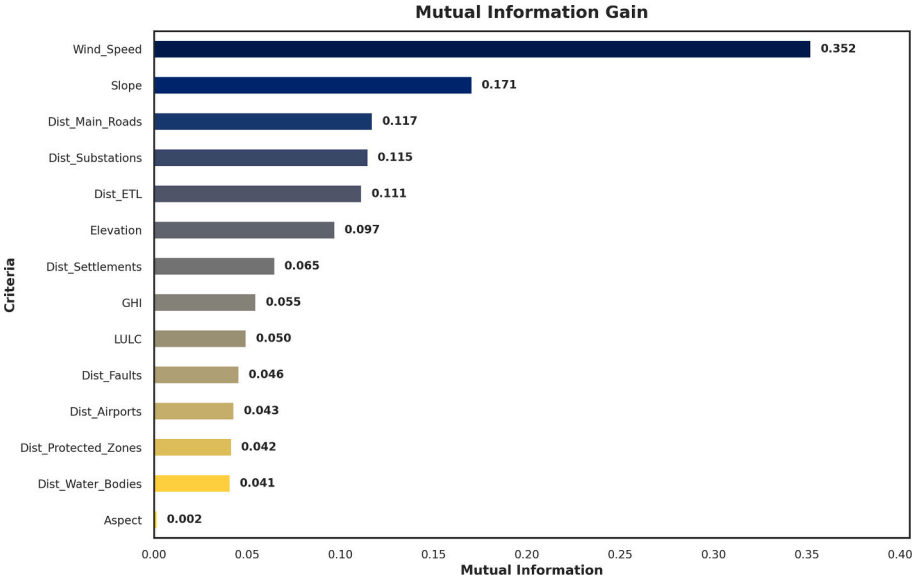

Fig. 8. MIG of the site selection criteria.

aspects, and Expert 4 emphasized Climatic and Topographic aspects. After aggregation, however, all four main criteria (Socio-Environmental, Economic, Climatic, and Topographic) received identical group weights (0.250) under both AHP and BWM (Appendix C). This balanced structure indicates that differences in suitability patterns are primarily driven by sub-criteria rather than by dominance of any main dimension, consistent with findings from other group-based MCDM studies [29].

Within the socio-environmental category, Distance to Protected Zones (AHP–BWM: 0.084–0.089) and LULC (0.084–0.085) received the highest weights, highlighting the importance of minimizing ecological impacts and land-use conflicts, in line with previous studies [12,23]. Distance to Airports received lower weights (0.042–0.040), reflecting its function mainly as a regulatory constraint rather than a continuous suitability driver [23]. In the climatic category, wind speed dominated (AHP–BWM: 0.169–0.164), consistent with its central role in wind and hybrid siting studies [12,17,19,22,23,28]. Within the topographic category, slope was the most influential criterion (0.176–0.185), whereas elevation received lower weights (0.062–0.063), indicating

Table 11
Weights for the sub-criteria.

	Expert 1		Expert 2		Expert 3		Expert 4		Expert 5		Group Decision	
	AHP	BWM	AHP	BWM	AHP	BWM	AHP	BWM	AHP	BWM	AHP	BWM
C1	0.094	0.083	0.101	0.099	0.090	0.090	0.062	0.050	0.073	0.104	0.084	0.085
C2	0.094	0.083	0.101	0.099	0.090	0.090	0.062	0.069	0.073	0.104	0.084	0.089
C4	0.028	0.028	0.035	0.033	0.048	0.036	0.062	0.069	0.038	0.032	0.042	0.040
C7	0.166	0.167	0.199	0.188	0.065	0.060	0.188	0.178	0.130	0.120	0.150	0.143
C8	0.166	0.167	0.092	0.099	0.151	0.145	0.059	0.069	0.130	0.120	0.120	0.120
C9	0.077	0.083	0.085	0.066	0.157	0.181	0.117	0.104	0.130	0.120	0.113	0.111
C11	0.166	0.167	0.176	0.177	0.183	0.181	0.176	0.178	0.145	0.120	0.169	0.164
C13	0.154	0.167	0.167	0.199	0.179	0.181	0.167	0.178	0.215	0.200	0.176	0.185
C15	0.055	0.056	0.044	0.040	0.036	0.036	0.108	0.104	0.067	0.080	0.062	0.063

Note: Since all main-criterion dimensions were considered equally important based on expert judgments, the sub-criterion weights were treated as global criterion weights.

that constructability constraints outweigh altitude effects [25]. Overall, AHP and BWM produced highly consistent weighting structures, and all consistency ratios remained within acceptable thresholds (Appendix D), confirming the reliability of expert judgments.

Alongside expert-based AHP and BWM weighting, an objective CRITICanalysis was applied to the continuous criteria. The categorical LULC criterion (C1) was excluded from CRITIC and instead assigned a fixed global weight equal to the mean of its AHP and BWM group weights $\beta \approx 0.085$. The remaining weight share $(1-\beta)$ was redistributed across continuous criteria according to their CRITIC scores, yielding the final hybrid weighting scheme (Table 12).

Under this scheme, C13 (0.247) and C15 (0.150) emerged as the most informative criteria, followed by C9 and C8. C1 retained a stable contribution (0.085), while C4 (0.084), C7 (0.082), C2 (0.080), and C11 (0.078) showed moderately differentiated influences on overall suitability. In contrast to many expert-driven studies where wind speed receives high weight, CRITIC assigned wind speed a comparatively low importance. This result highlights the value of objective weighting in revealing the true discriminative power of criteria under region-specific conditions, where renewable resources are relatively homogeneous and topographic and infrastructural factors provide greater differentiation.

4.4. Results of the site suitability assessments

4.4.1. Results of the sensitivity analysis of AHP, BWM, and CRITIC

Sensitivity analysis was conducted to assess the robustness of suitability outputs under uncertainty in criterion weights. A one-at-a-time perturbation approach was applied, whereby each weight was independently adjusted by ±10% and remaining weights were rescaled to preserve the unit-sum constraint, consistent with established GIS-MCDM practice [70]. Robustness was evaluated using two complementary indicators: Spearman's rank correlation coefficient to assess ranking stability, and the Jaccard similarity index to assess spatial stability of the top 5%, 10%, and 20% most suitable areas.

For each weighting method (AHP, BWM, and CRITIC), baseline suitability scores were first computed, followed by recalculation under perturbed weight scenarios. Across all criteria and methods, Spearman correlation coefficients remained extremely high ($\rho \approx 0.999$–1.000), indicating near-perfect preservation of ranking order and low sensitivity to moderate weight variation.

Spatial robustness analysis further confirmed high stability. Jaccard similarity values ranged from approximately 94.7% to 98.7% across all criteria and weighting methods (Fig. 9). Wind speed, elevation, distance to protected zones, and distance to energy transmission lines exhibited the highest stability, while slope and LULC showed slightly lower—but still very high—overlap. CRITIC demonstrated spatial stability comparable to, and in some cases marginally higher than, AHP and BWM. Overall, these results indicate that suitability patterns are largely insensitive to moderate weight uncertainty, confirming the robustness of the proposed GIS-MCDM framework for practical planning applications.

Table 12
Weights for the CRITIC method.

	Variance	Information content	Mean absolute correlation	Discriminative power	Weight
C13	0.070	0.248	0.206	0.794	0.247
C15	0.053	0.188	0.368	0.632	0.150
C9	0.029	0.101	0.195	0.805	0.102
C8	0.032	0.111	0.345	0.655	0.092
C1	–	–	–	–	0.085
C4	0.031	0.109	0.385	0.615	0.084
C7	0.024	0.083	0.213	0.787	0.082
C2	0.027	0.094	0.327	0.673	0.080
C11	0.019	0.066	0.068	0.932	0.078

4.4.2. Spatial autocorrelation and spatially adjusted comparison of suitability values

Since SSMs constitute spatially continuous surfaces, independence among pixel-based observations may be violated. Spatial autocorrelation was therefore quantified prior to statistical comparison. Global Moran's I, computed over 47,039 valid raster cells, indicated strong positive spatial dependence for all suitability maps (AHP: $I = 0.8245$; BWM: $I = 0.8003$; CRITIC: $I = 0.6801$; $p_{sim} = 0.001$), and for all difference maps (AHP–BWM: $I = 0.8753$; AHP–CRITIC: $I = 0.7184$; BWM–CRITIC: $I = 0.7475$; $p_{sim} = 0.001$).

Accordingly, spatially adjusted paired *t*-tests using effective sample sizes were applied. All pairwise comparisons remained statistically significant: AHP–BWM ($n_{eff} = 3129$, mean difference $= 0.0591$, $t = 38.63$, $p < 0.001$), confirmed by a Monte Carlo permutation test ($p_{perm} = 0.0001$). Similarly, significant differences were observed for AHP–-CRITIC ($n_{eff} = 7710$; mean $= 0.1916$; $t = 50.99$, $p < 0.001$; $p_{perm} = 0.0001$) and BWM–CRITIC ($n_{eff} = 6798$; mean $= 0.1325$; $t = 29.58$, $p < 0.001$; $p_{perm} = 0.0001$). Even after explicitly accounting for spatial dependence, differences among AHP-, BWM-, and CRITIC-based suitability patterns remain statistically significant, demonstrating the robustness of the comparative weighting framework.

4.4.3. SSMs and suitability patterns

SSMs generated using AHP, BWM, and CRITIC within the weighted-sum framework are presented in Fig. 10, and the areal distribution of suitability classes is summarized in Table 13. Visual comparison indicates that the three SSMs assign different suitability levels to the same locations. The analysis reveals that extensive areas of Izmir Province are classified as highly or very highly suitable for hybrid energy system implementation (Fig. 10). Areal statistics confirm substantial variation among methods. Under AHP, 27.89% and 5.38% of candidate areas are classified as “High” and “Very High” suitability, respectively, compared with 23.12% and 4.63% under BWM. In contrast, CRITIC assigns markedly larger proportions to these classes (48.46% and 9.93%). Conversely, the proportions of “Low” and “Very Low” suitability are

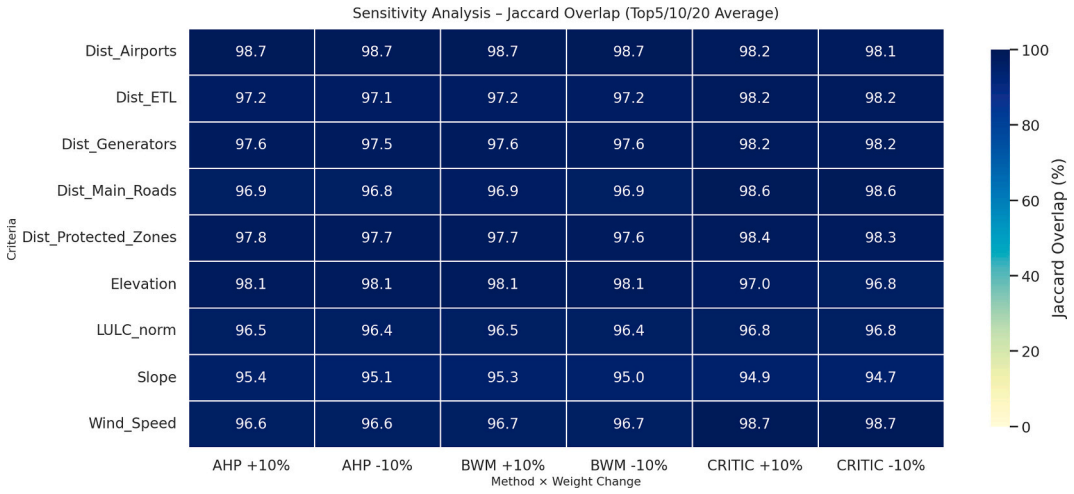

Fig. 9. Jaccard Similarity Results (Average of Top 5/10/20%).

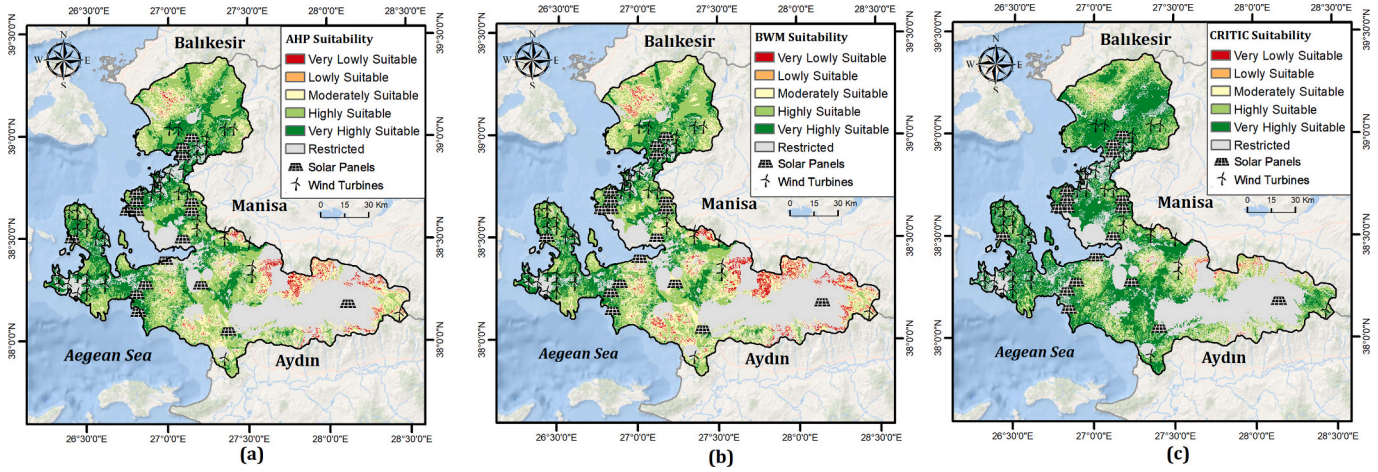

Fig. 10. SSMs for the study region (a): AHP, (b): BWM, (c): CRITIC.

Table 13
Areal distribution of the suitability levels.

Suitability Degree	AHP (%)	BWM (%)	CRITIC (%)
Very lowly	2.93	4.87	0.60
Lowly	20.36	25.46	10.28
Moderately	43.44	41.92	30.73
High	27.89	23.12	48.46
Very High	5.38	4.63	9.93

23.29% (AHP), 30.33% (BWM), and 10.88% (CRITIC). These percentages refer only to candidate areas, as restricted locations were excluded based on the thresholds in Table 4.

The resulting SSMs provide spatially explicit decision-support for planners and energy stakeholders by identifying undeveloped areas suitable for hybrid energy deployment. The maps can support strategic planning aimed at maximizing renewable energy potential while potentially reducing siting conflicts and project costs in Izmir Province.

To validate the SSMs, existing SPV and WT locations were overlaid with the derived suitability maps. Installation locations were compiled from OpenStreetMap and cross-checked with publicly available institutional datasets and high-resolution aerial imagery to improve positional accuracy and completeness. After excluding restricted areas, 703 installations were evaluated. Across all methods, most installations were located within the High and Very High suitability classes, although class dominance varied by method (Table 14). Under AHP, 77.81% of installations fell within the High/Very High classes, compared with 72.83% under BWM and 83.65% under CRITIC. The Moderately suitable class accounted for a smaller proportion of installations (AHP: 12.95%, BWM: 16.36%, CRITIC: 6.97%), while the Lowly suitable class remained negligible (AHP: 0.42%, BWM: 1.99%, CRITIC: 0.56%). Additionally, 59 installations (8.82%) overlapped with restricted areas, primarily due to low wind speed (< 4.4 m/s), steep slopes (> 25%), high elevations (> 1250 m), and buffer constraints around protected areas and airports. This outcome is expected because exclusion was applied under an "AND" rule, whereby exceeding any single threshold classified a site as restricted.

4.4.4. *Results of the clustering and suitability polygon generation*

SSMs are useful for identifying promising areas but they do not

Table 14
Distribution of existing SPV/WT facilities by suitability class.

Suitability Class	AHP (%)	BWM (%)	CRITIC (%)
Very Low	–	–	–
Low	0.42	1.99	0.56
Moderate	12.95	16.36	6.97
High	53.63	49.93	44.52
Very High	24.18	22.90	39.13
Restricted	8.82	8.82	8.82

provide explicit site boundaries. To address this limitation, HDBSCAN clustering was applied to locations with suitability ≥4 to delineate spatially coherent candidate zones. HDBSCAN parameters were optimized using a grid-search–like procedure, maximizing Silhouette [79], Calinski–Harabasz [80], and minimizing Davies–Bouldin [81] indices, while constraining the maximum cluster size to 100 pixels (Appendix E). The optimized configuration produced 103 clusters. Clustering quality was high (Silhouette = 0.6683; Calinski–Harabasz = 347,148.15; Davies–Bouldin = 0.4921). Cluster sizes ranged from 40 to 100 pixels (mean = 63; median = 59), satisfying the imposed size constraint. Approximately 83.33% of points were classified as noise, indicating that many suitable locations were spatially isolated under the optimized density criteria. Clusters were subsequently converted into site suitability polygons using the Concave Hull algorithm. Due to the absence of validation data for hybrid facilities, polygon quality was assessed visually to ensure that boundaries did not extend beyond the study area or into restricted zones.

4.4.5. Ranking results of the suitability polygons

A key gap in renewable energy siting studies is the lack of systematic prioritization of suitable locations based on investment potential; most studies rely on visual interpretation rather than algorithmic ranking due to the large number of pixels involved. In this study, the delineation of site suitability polygons enables site-level prioritization. Mean criterion values were computed for each polygon and combined with criterion weights using the TOPSIS and MABAC methods. The resulting positive and negative ideal solutions are reported in Table 15. Criteria C1, C2, C4, and C11 were treated as benefit criteria, whereas C7, C8, C9, C13, and C15 were treated as cost criteria.

The distances to the positive and negative ideal solutions (S^+ and S^-), relative closeness values (C), and rankings of the top 10 candidate sites are reported in Table 16. Most sites exhibit moderate proximity to the ideal solution ($C > 0.5$). The highest closeness value ($C = 0.8948$) indicates strong but not perfect performance across criteria, consistent with the expectation that no single site optimizes all criteria simultaneously.

To further assess the robustness of polygon prioritization, MABAC was applied as a complementary ranking method under the same settings. Positive MABAC scores (Q_i) indicate alternatives above the border approximation area (more suitable), whereas negative values indicate lower suitability. The MABAC rankings (Table 17) broadly align with TOPSIS, with minor differences in site ordering. MABAC tended to prioritize some neighboring polygons while excluding some more distant sites, indicating that it can serve as a complementary method for capturing additional high-priority areas.

Cross-method agreement between TOPSIS and MABAC was evaluated for the Top-10 shortlisted polygons ($N = 10$) to assess whether the additional framework components yield meaningful differences beyond a single ranking method. The two methods shared 7 of 10 sites (Top-10 overlap = 70%; Jaccard = 0.538), defining a consensus subset of robust candidates. However, the ordering of shared sites differed substantially (Spearman $\rho = 0.107$; $n = 7$), indicating that while shortlist composition is relatively stable, within-list prioritization is method-sensitive. These findings complement the sensitivity analysis by distinguishing robustness to weight uncertainty (ρ ≈ 0.999–1.000; Jaccard ≈ 94.7–98.7%) from ranking-method dependence at the site-prioritization stage.

Selected suitability polygons identified by agreement between TOPSIS and MABAC are shown in Fig. 11. These polygons largely coincide with areas classified as High or Very High suitability, indicating strong internal consistency between the suitability mapping and ranking stages. Their spatial distribution shows that candidate sites are distributed across the study region rather than clustered in only a few locations.

Unlike many GIS–MCDM studies where polygons are manually delineated or visually aggregated (Table 1), the polygons presented here are generated algorithmically through integrated clustering and polygonization. This improves objectivity, reproducibility, and reduces analyst-dependent bias. The resulting polygons provide clear spatial extents suitable for preliminary planning and screening-level decision-making. Nonetheless, their boundaries should be refined through site-specific assessments, as land-use conflicts, regulatory constraints, or model uncertainty may affect real-world feasibility.

Table 15
The positive (A^+) and negative (A^-) ideal solution values.

Criterion	A^+	A^-
C15	0.0001	0.0237
C11	0.0299	0.0192
C13	0.0078	0.0425
C9	0.0024	0.0623
C4	0.0096	0.0009
C8	0.0002	0.1012
C7	0.0020	0.0634
C2	0.0225	0.0014
C1	0.0219	0.0005

Table 16
The distances to positive and negative ideal solutions and ranking of the suitable sites for top ten sites

Site ID	S_i^+	S_i^-	C_i	Ranking
36	0.0161	0.1371	0.8948	1
51	0.0165	0.1393	0.8938	2
49	0.0179	0.1300	0.8788	3
30	0.0212	0.1349	0.8642	4
29	0.0210	0.1304	0.8612	5
25	0.0219	0.1331	0.8589	6
40	0.0214	0.1304	0.8588	7
45	0.0216	0.1289	0.8565	8
43	0.0230	0.1338	0.8531	9
26	0.0228	0.1308	0.8518	10

Table 17
MABAC-based final scores and ranking of the top ten suitable sites.

Site ID	Final Score (Q_i)	Rank	Interpretation
48	0.1835	1	Above BAA (Good)
40	0.1774	2	Above BAA (Good)
47	0.1748	3	Above BAA (Good)
49	0.1571	4	Above BAA (Good)
36	0.1527	5	Above BAA (Good)
51	0.1455	6	Above BAA (Good)
29	0.1436	7	Above BAA (Good)
13	0.1241	8	Above BAA (Good)
30	0.1238	9	Above BAA (Good)
25	0.1227	10	Above BAA (Good)

4.5. Limitations and future research directions

This study has several limitations that also highlight directions for future research. First, reliance on openly available spatial datasets enhances transparency and reproducibility but introduces uncertainties related to data completeness and accuracy. In particular, OpenStreetMap inventories of existing WT and SPV installations may contain positional or coverage errors that can affect validation and candidate-site identification. Future work would benefit from incorporating higher-resolution and officially validated datasets, especially for wind speed and GHI, which currently have coarser spatial resolution than several other criteria.

Second, the framework was applied only to Izmir Province. Although the results demonstrate methodological feasibility and practical relevance, empirical transferability to other regions remains untested. Nevertheless, the framework is inherently adaptable due to its modular design, use of widely available datasets, and flexible weighting schemes.

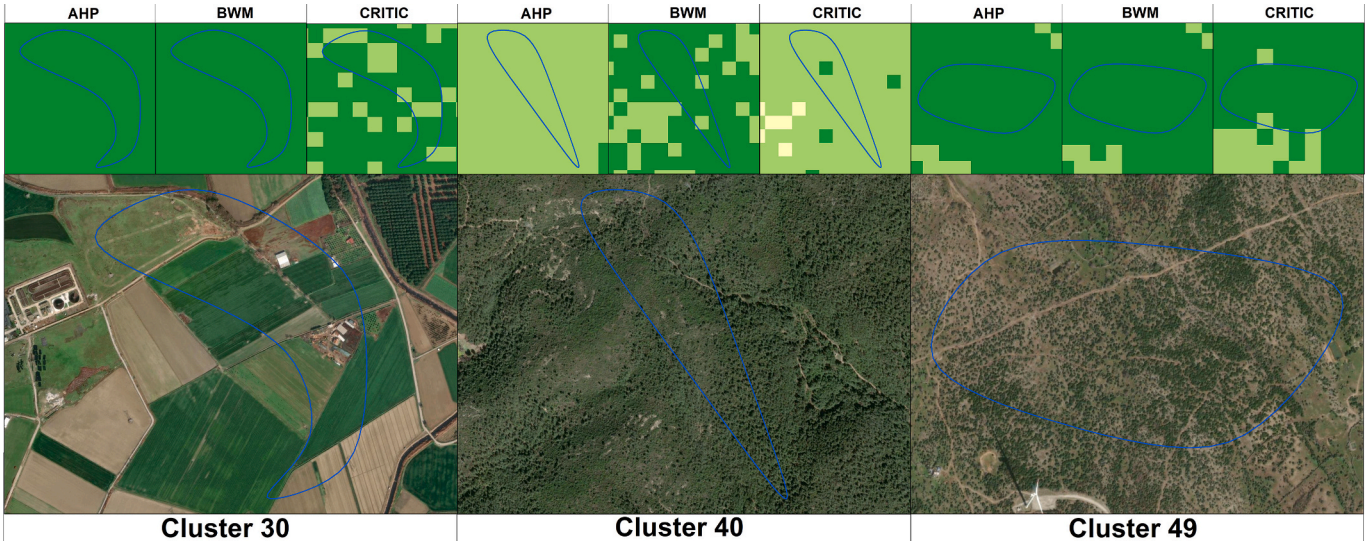

Fig. 11. Proposed suitability polygons for AHP, BWM, and CRITIC with corresponding real-world site appearances.

Future studies should evaluate its performance across regions with differing environmental, socio-economic, and regulatory conditions, as criterion importance in GIS–MCDM applications is inherently context-dependent.

Third, solar-resource variability within the feasible domain of Izmir Province is low; consequently, SPV functions primarily as an adequacy baseline, while wind and non-climatic constraints drive most spatial differentiation among candidate sites. This pattern reflects a regional characteristic. In regions with stronger solar gradients, the same framework would be expected to retain GHI during feature selection and to yield more balanced hybrid differentiation. In this context, objective and fully data-driven weighting methods such as CRITIC offer a promising pathway for reducing subjectivity and improving cross-regional comparability. Transferability could be further strengthened by integrating fully data-driven ML models, provided that reliable and comprehensive ground-truth data on hybrid energy facilities become available.

Finally, the spatial exclusion thresholds adopted in this study were derived primarily from Turkish regulations and established practices. While these values ensure national regulatory consistency, the proposed workflow is modular: exclusion layers and setback distances can be re-parameterized for other regulatory contexts without altering the core framework. Nevertheless, the lack of universally accepted standards for spatial restrictions necessitates careful contextual validation, potentially supported by structured expert judgment. Moreover, socio-economic and market factors—such as land ownership, grid capacity, investment incentives, and public acceptance—were not explicitly modeled and should be incorporated in future applications to enhance policy relevance.

5. Conclusions

The environmental and public health risks associated with fossil fuel use increasingly highlight the potential of hybrid SPV–WT systems to deliver more reliable and balanced energy generation through temporal complementarity. However, site selection for such systems remains a complex task requiring the integrated evaluation of socio-environmental, economic, climatic, and topographic constraints.

This study proposes an integrated GIS–MCDM–ML framework for Izmir Province to address three key gaps in the literature: (i) the lack of statistical comparison across alternative weighting methods, (ii) the absence of data-driven criterion selection prior to weighting, and (iii) the predominant reliance on raster-based outputs without polygonization and investment-oriented prioritization.

Within the proposed framework, criterion weights were derived using expert-based methods (AHP and BWM) alongside an objective, data-driven method (CRITIC); exclusion constraints were applied based on national legislation and prior literature; the criterion set was refined using ML-based feature selection and statistical testing; suitability maps were generated in a GIS environment; both criterion weights and resulting suitability patterns were evaluated through comprehensive sensitivity analysis; and high-suitability areas were clustered using HDBSCAN, converted into polygons, and prioritized using ranking-based MCDM methods (TOPSIS and MABAC).

The main findings of the proposed framework are summarized as follows:

- Of the initial 15 criteria, 9 were retained after statistical evaluation and feature selection.
- The SSMs derived from AHP, BWM, and CRITIC exhibited strong positive spatial autocorrelation and were compared using spatially adjusted *t*-tests, revealing statistically significant differences among all three weighting methods.
- Under the AHP-based SSM, 33.27% of the study area was classified as highly or very highly suitable, compared with 27.75% for BWM and 58.39% for CRITIC
- A large proportion of existing SPV and WT installations fell within high-suitability classes (AHP: 77.81%, BWM: 72.83%, CRITIC: 83.65%), confirming the reliability of the proposed framework.
- HDBSCAN clustering identified 103 potential candidate zones, achieving a Silhouette score of 0.6683, a Calinski–Harabasz score of 347,148.15, and a Davies–Bouldin index of 0.4921, indicating well-defined and compact clusters.
- Polygonization produced candidate areas with clear spatial boundaries, all of which were ranked, and the top 10 zones were reported for investment prioritization using TOPSIS and MABAC.
- Several high-priority zones with no existing renewable energy facilities were identified, highlighting promising opportunities for future development.

From a policy and practical perspective, the proposed framework provides actionable decision support for grid and transmission planning, environmental risk mitigation, and investment prioritization, while ensuring objectivity, transparency, and reproducibility. The framework therefore supports the low-carbon energy transition in alignment with the Paris Agreement and the United Nations Sustainable Development

Goals (SDG 7 and SDG 13). Overall, the results demonstrate strong potential for scaling the framework to regional or national levels and for supporting policymakers, regulators, and investors in identifying priority zones for hybrid renewable energy siting.

Declaration of generative AI and AI-assisted technologies in the manuscript preparation process

During the preparation of this work, the authors used ChatGPT (GPT-5.2) for proofreading. After using this tool, the authors reviewed and edited the content as needed and take full responsibility for the content of the publication.

CRediT authorship contribution statement

Yasin Ferit Uguz: Writing – original draft, Visualization, Validation, Software, Methodology, Investigation, Formal analysis, Data curation. **Atakan Bilgili:** Writing – review & editing, Writing – original draft, Validation, Supervision, Software, Project administration, Methodology, Investigation, Formal analysis, Data curation, Conceptualization. **Melis Uzar:** Writing – review & editing, Supervision, Project administration, Investigation, Conceptualization.

Declaration of competing interest

The authors declare that they have no known competing financial interests or personal relationships that could have appeared to influence the work reported in this paper.

Appendix A. Initial weights for AHP & BWM

Criteria Type	Main Criteria	Sub Criteria	BWM Weight	AHP Weight
Socio-Environmental	Land Use	Not Suitable	0.393%	0.293%
		Less Suitable	0.774%	0.570%
		Moderately Suitable	1.083%	1.129%
		Suitable	1.806%	2.187%
		High Suitable	4.475%	4.227%
	Distance to Protected Zones	500–1000	0.411%	0.293%
		1000-3000	0.810%	0.570%
		3000–5000	1.134%	1.129%
		5000-7000	1.890%	2.187%
		>7000	4.683%	4.227%
	Distance to Airports	3000-7000	0.183%	0.147%
		7000–14,000	0.360%	0.285%
		14,000-21,000	0.504%	0.566%
		21,000-28,000	0.840%	1.096%
		>28,000	2.081%	2.118%
Economic	Distance to Main Roads	0–100	0.656%	0.520%
		100–1000	7.478%	7.515%
		1000-3000	3.017%	3.889%
		3000–5000	1.810%	2.008%
		>5000	1.293%	1.013%
	Distance to Energy Transmission Lines	0–1000	6.294%	6.015%
		1000-4000	2.540%	3.113%
		4000-7000	1.524%	1.607%
		7000–10,000	1.088%	0.811%
		>10,000	0.552%	0.417%
	Distance to Substations	250–5000	5.815%	5.692%
		5000–10,000	2.346%	2.946%
		10,000–15,000	1.408%	1.521%
		15,000-20,000	1.006%	0.767%
		>20,000	0.510%	0.394%
	Wind Speed	4.4–5.0	0.757%	0.589%
		5.0–5.5	1.492%	1.147%
		5.5–6.0	2.088%	2.274%
		6.0–6.5	3.481%	4.405%
		>6.5	8.626%	8.512%
Topographic	Slope	0–5	9.697%	8.866%
		5–10	3.913%	4.589%
		10–15	2.348%	2.369%
		15–20	1.677%	1.195%
		20–25	0.851%	0.614%
	Elevation	0–250	3.309%	3.111%
		250–500	1.335%	1.610%
		500–750	0.801%	0.831%
		750–1000	0.572%	0.419%
		1000–1250	0.290%	0.215%

Appendix B

Table A1
Annual GHI variability in the full study area vs feasible area (constraints applied).

Domain	mean (kWh/m^2/yr)	std (kWh/m^2/yr)	CV (%)	min (kWh/m^2/yr)	max (kWh/m^2/yr)
Full study area	1750.96	46.79	2.672	1426.06	1838.14
Feasible area (constraints applied)	1747.94	47.58	2.722	1426.06	1838.14

Table A2
Annual wind-speed variability in the full study area vs feasible area (constraints applied).

Domain	mean (m/s)	std (m/s)	CV (%)	min (m/s)	max (m/s)
Full study area	6.27187	1.66067	26.478	2.033	13.7
Feasible area (constraints applied)	6.81481	1.28525	18.86	4.4	13.7

Appendix C. Weights for the main criteria

	Expert 1	Expert 2	Expert 3	Expert 4	Expert 5	Group Decision
Socio-Environmental	0,2500	0,3333	0,2500	0,1667	0,2500	0,2500
Economic	0,2500	0,3333	0,2500	0,1667	0,2500	0,2500
Climatic	0,2500	0,1667	0,2500	0,3333	0,2500	0,2500
Topographic	0,2500	0,1667	0,2500	0,3333	0,2500	0,2500

Appendix D. CR Values For 9 Criteria

Expert	CR (AHP)	CR (BWM)
Expert 1	1.12%	0.00%
Expert 2	1.12%	3.33%
Expert 3	2.50%	0.00%
Expert 4	0.72%	16.67%
Expert 5	0.76%	5.00%

Appendix E. The dictionary for the clustering optimization

Parameter	Dictionary
“min_cluster_size”	{10, 20, 40}
“min_samples”	{5, 10,20}
“cluster_selection_epsilon”	{10, 20, 30, 40, 50}
“max_cluster_size”	{50,100,200}
chosen best parameters	“min_cluster_size”: 40, “min_samples”: 20, “cluster_selection_epsilon”: 10, “max_cluster_size”: 100

Data availability

Data will be made available on request.

References

[1] International Energy Agency (IEA). Global Energy Review 2025: Key findings 2025, https://www.iea.org/reports/global-energy-review-2025/key-findings (accessed 01 Dec 2025).

[2] International Energy Agency. World Energy Outlook 2022:2022. https://www.iea.org/reports/world-energy-outlook-2022 (accessed 02 May 2025).

[3] European Commission. REPowerEU: A plan to rapidly reduce dependence on Russian fossil fuels and fast forward the green transition. 17 May 2022, https://ec.europa.eu/commission/presscorner/detail/en/ip_22_3131 (accessed 18 Jun 2025).

[4] Martins F, Felgueiras C, Smitkova M, Caetano N. Analysis of fossil fuel energy consumption and environmental impacts in European countries. Energies 2019;12(6):964. https://doi.org/10.3390/en12060964.

[5] Perera F. Pollution from fossil-fuel combustion is the leading environmental threat to global pediatric health and equity: solutions exist. Int J Environ Res Public Health 2017;15(1):16. https://doi.org/10.3390/ijerph15010016.

[6] Health Effects Institute; Institute for Health Metrics and Evaluation. State of Global Air. A special report on global exposure to air pollution and its health impacts, with a focus on children's health 2024:2024. https://www.stateofglobalair.org/sites/default/files/documents/2024-06/soga-2024-report_0.pdf (accessed 27 May 2025).

[7] Asheim G, Fæhn T, Nyborg K, Greaker M, Hagem C, Harstad B, et al. The case for a supply-side climate treaty. Science 2019;365:325–7. https://doi.org/10.1126/science.aax5011.

[8] Ember. Global Electricity Review 2023. 12 Apr 2023, https://ember.energy/insights/research/global-electricity-review-2023/ (accessed 07 May 2025).

[9] Fetting C. The European green Deal. ESDN. Report 2020. https://www.esdn.eu/fileadmin/ESDN_Reports/ESDN_Report_2_2020.pdf [accessed 29 May 2025].

[10] Latinopoulos D, Kechagia K. A GIS-based multi-criteria evaluation for wind farm site selection: a regional-scale application in Greece. Renew Energy 2015;78:550–60. https://doi.org/10.1016/j.renene.2015.01.041.

[11] Elkadeem M, Younes A, Sharshir S, Campana P, Wang S. Sustainable siting and design optimization of hybrid renewable energy system: a geospatial multi-criteria

analysis. Appl Energy 2021;295:117071. https://doi.org/10.1016/j.apenergy.2021.117071.
[12] Tercan E. Land suitability assessment for wind farms through best-worst method and GIS in Balıkesir province of Turkey. Sustain Energy Technol Assess 2021;47:101491. https://doi.org/10.1016/j.seta.2021.101491.
[13] Uyan M. GIS-based solar farms site selection using analytic hierarchy process (AHP) in Karapınar region, Konya/Turkey. Renew Sustain Energy Rev 2013;28:11–7. https://doi.org/10.1016/j.rser.2013.07.042.
[14] Janke J. Multicriteria GIS modeling of wind and solar farms in Colorado. Renew Energy 2010;35:2228–34. https://doi.org/10.1016/j.renene.2010.03.014.
[15] Rezaei J. Best-worst multi-criteria decision-making method. Omega 2015;53:49–57. https://doi.org/10.1016/j.omega.2014.11.009.
[16] Chaibi M, Ben Ghoulam EM, Khallouk N, et al. A novel fuzzy-multi-criteria-GIS-machine learning approach for onshore wind power plant site selection. Euro-Mediterr J Environ Integr 2025;10:1025–45. https://doi.org/10.1007/s41207-024-00653-6.
[17] Şahin G, Koç A, Doğan S, Rüstemli S, van Sark W. Exploring of wind energy potential and optimal site selection for wind energy plants installations in Erzurum/Turkey based on multicriteria site selection. Int J Energy Res 2025. https://doi.org/10.1155/er/2629977.
[18] Yildiz SS. Spatial multi-criteria decision-making approach for wind farm site selection: a case study in Balıkesir. Turkey Renew Sustain Energy Rev 2024;192:114158. https://doi.org/10.1016/j.rser.2023.114158.
[19] Yaman A. A GIS-based multi-criteria decision-making approach (GIS-MCDM) for determination of the most appropriate site selection of onshore wind farm in Adana, Turkey. Clean Technol Environ Policy 2024. https://doi.org/10.1007/s10098-024-02866-3.
[20] Bilgili A, Arda T, Kılıç B. Explainability in wind farm planning: a machine learning framework for automatic site selection of wind farms. Energ Conver Manage 2024;309:118441. https://doi.org/10.1016/j.enconman.2024.118441.
[21] Kocabaldır C, Yücel MA. GIS-based multi-criteria decision analysis of site selection for photovoltaic power plants in Çanakkale Province. Int J Environ Geoinformatics 2020;7(3):347–55. https://doi.org/10.30897/ijegeo.689570.
[22] Zalhaf AS, Elboshy B, Kotb KM, Han Y, Almaliki AH, Aly RMH, et al. A high-resolution wind farms suitability mapping using GIS and fuzzy AHP approach: a national-level case study in Sudan. Sustainability 2022;14(1):358. https://doi.org/10.3390/su14010358.
[23] Saraswat SK, Digalwar AK, Yadav SS, Kumar G. MCDM and GIS-based modelling technique for assessment of solar and wind farm locations in India. Renew Energy 2021;169:865–84. https://doi.org/10.1016/j.renene.2021.01.056.
[24] Cunden TSM, Doorga J, Lollchund MR, Rughooputh SDDV. Multi-level constraints wind farms siting for a complex terrain in a tropical region using MCDM approach coupled with GIS. Energy 2020;211:118533. https://doi.org/10.1016/j.energy.2020.118533.
[25] Soydan O. Solar power plants site selection for sustainable ecological development in Nigde, Turkey. SN Appl Sci 2021;3:41. https://doi.org/10.1007/s42452-020-04112-z.
[26] Giamalaki M, Tsoutsos T. Sustainable siting of solar power installations in Mediterranean using a GIS/AHP approach. Renew Energy 2019;141:64–75. https://doi.org/10.1016/j.renene.2019.03.100.
[27] Merrouni AA, Elwali Elalaoui F, Mezrhab A, Mezrhab A, Ghennioui A. Large-scale PV sites selection by combining GIS and analytical hierarchy process: case study eastern Morocco. Renew Energy 2018;119:863–73. https://doi.org/10.1016/j.renene.2017.10.044.
[28] Ali S, Taweekun J, Techato K, Waewsak J, Gyawali S. GIS-based site suitability assessment for wind and solar farms in Songkhla, Thailand. Renew Energy 2019;132:1360–72. https://doi.org/10.1016/j.renene.2018.09.035.
[29] Ayodele TR, Ogunjuyigbe ASO, Odigie O, Munda JL. A multi-criteria GIS-based model for wind farm site selection using interval type-2 fuzzy analytic hierarchy process: the case study of Nigeria. Appl Energy 2018;228:1853–69. https://doi.org/10.1016/j.apenergy.2018.07.051.
[30] Türkiye İstatistik Kurumu (TÜİK). Adrese Dayalı Nüfus Kayıt Sistemi Sonuçları 2022, https://data.tuik.gov.tr/bulten/index?p=adrese-dayali-nufus-kayit-sistemi-sonuclari-2022-49685 (accessed 03 Jun 2025).
[31] Ozay C, Celiktas MS. Statistical analysis of wind speed using two-parameter Weibull distribution in Alaçatı region. Energ Conver Manage 2016;121:49–54. https://doi.org/10.1016/j.enconman.2016.05.026.
[32] Gungor A, Gokcek M, Uçar H, Arabacı E, Akyüz A. Analysis of wind energy potential and Weibull parameter estimation methods: a case study from Turkey. Int J Environ Sci Technol 2019. https://doi.org/10.1007/s13762-019-02566-2.
[33] Sogukpinar H, Bozkurt I, Çağ S. Experimental and numerical analysis of solar potential and feed-in tariff in Turkey. In: 2016 IEEE International Conference on Power and Renewable Energy (ICPRE). 2016. https://doi.org/10.1109/ICPRE.2016.7871145. 594–597.
[34] Alain B, Yilanci A. Techno-economic analysis of 1 MWe solar power plant using combined Rankine cycle in Izmir, Turkey. Int J Energy Smart Grid 2018;3(2). https://doi.org/10.23884/IJESG.2018.3.2.01.
[35] Enerji Atlası, https://www.enerjiatlasi.com/ (accessed 21 Jun 2025).
[36] European Environment Agency. CORINE Land Cover dataset 2018:2018. https://doi.org/10.2909/960998c1-1870-4e82-8051-6485205ebbac.
[37] OpenStreetMap contributors. Planet dump 2024. https://www.openstreetmap.org [accessed 04 Jul 2025].
[38] European Space Agency. WorldCover 10 m v200. 2021, https://worldcover2020.esa.int/ (accessed 17 Jul 2025).
[39] General Directorate of Mineral Research and Exploration of Türkiye (MTA). Active Fault Map of Türkiye. 2024, https://www.mta.gov.tr/ (accessed 23 Apr 2025).
[40] World Bank Group. Global Solar Atlas. 2024, https://globalsolaratlas.info/ (accessed 05 Aug 2025).
[41] Technical University of Denmark (DTU). Global Wind Atlas 2024. https://globalwindatlas.info/ [accessed 14 Aug 2025].
[42] United States geological survey (USGS). Shuttle radar topography Mission (SRTM). Digital Elevation Model 2024. https://www.usgs.gov/ [accessed 26 May 2025].
[43] Ministry of Environment. Urbanization and climate change. Türkiye: Post-revision finalization document. Ankara; 2022. Available from: https://webdosya.csb.gov.tr/db/tabiat/icerikler/res-deg-s-kl-lk-sonrasi-20220802145655.pdf.
[44] Ministry of Agriculture and Forestry. Tahtalı Dam Basin protection plan. Published in the Official Gazette on 2017;Issue No. 30224. Available from: https://www.tarimorman.gov.tr/SYGM/Belgeler/havza%20koruma%20eylem%20planlar%C4%B1/Tahtali+Baraji+Havza+Koruma+Plani.pdf.
[45] Directorate General of Civil Aviation (SHGM). Regulation on obstacle criteria for communication, navigation and surveillance (CNS) systems. Published in the Official Gazette on 2012;Issue No. 28451. Available from: https://web.shgm.gov.tr/doc5/cns-mania.pdf.
[46] Urfalı T, Eymen A. CBS ve AHP yöntemi yardımıyla Kayseri ili örneğinde rüzgâr enerji santrallerinin yer seçimi. Geomatik 2021;6(3):227–37. https://doi.org/10.29128/geomatik.772453.
[47] Noorollahi Y, Ghenaatpisheh Senani A, Fadaei A, Simaee M, Moltames R. A framework for GIS-based site selection and technical potential evaluation of PV solar farm using fuzzy-Boolean logic and AHP multi-criteria decision-making approach. Renew Energy 2022;186:89–104. https://doi.org/10.1016/j.renene.2021.12.124.
[48] Gigović L, Pamučar D, Božanić D, Ljubojević S. Application of the GIS-DANP-MABAC multi-criteria model for selecting the location of wind farms: a case study of Vojvodina, Serbia. Renewable Energy 2017;103:501–21. https://doi.org/10.1016/j.renene.2016.11.057.
[49] Moradi S, Yousef H, Noorollahi Y, Rosso D. Multi-criteria decision support system for wind farm site selection and sensitivity analysis: case study of Alborz Province. Iran Energy Strategy Rev 2020;29:100478. https://doi.org/10.1016/j.esr.2020.100478.
[50] Noorollahi Y, Yousef H, Mohammadi M. Multi-criteria decision support system for wind farm site selection using GIS. Sustain Energy Techn and Assess 2016;13:38–50. https://doi.org/10.1016/j.seta.2015.11.007.
[51] Ryberg D, Robinius M, Stolten D. Evaluating land eligibility constraints of renewable energy sources in Europe. Energies 2018;11(5):1246. https://doi.org/10.3390/en11051246.
[52] Rehbein JA, Watson JEM, Lane JL, et al. Renewable energy development threatens many globally important biodiversity areas. Glob Change Biol 2020. https://doi.org/10.1111/gcb.15067.
[53] Auld T, McHenry MP, Whale J. US military, airspace, and meteorological radar system impacts from utility-class wind turbines: implications for renewable energy targets and the wind industry. Renew Energy 2013;55:24–30. https://doi.org/10.1016/j.renene.2012.12.008.
[54] Swan S, Hadjian AH. The 1986 North Palm Springs earthquake: Effects on power facilities. NP-5607 Research Project 2848. Palo Alto: Electric Power Research Institute; 1988.
[55] Al Garni HZ, Awasthi A. Solar PV power plant site selection using a GIS-AHP based approach with application in Saudi Arabia. Appl Energy 2017;206:1225–40. https://doi.org/10.1016/j.apenergy.2017.10.024.
[56] Rusek S, Strida F, Mach M. The problems of electrical distance in connection with the operation of wind power generator. In: 2010 9th International Conference on Environment and Electrical Engineering. 2010. https://doi.org/10.1109/EEEIC.2010.5490014.
[57] Halinka A, Szewczyk M. Distance protections in the power system lines with connected wind farms. In: From Turbine to Wind Farms—Technical Requirements and Spin-Off Products. InTech; 2011. https://doi.org/10.5772/15955.
[58] Yang H, Wei Z, Chengzhi L. Optimal design and techno-economic analysis of a hybrid solar–wind power generation system. Appl Energy 2009;86(2):163–9. https://doi.org/10.1016/j.apenergy.2008.03.008.
[59] Zoghi M, Ehsani AH, Sadat M, Amiri MJ, Karimi S. Optimization solar site selection by fuzzy logic model and weighted linear combination method in arid and semi-arid region: a case study Isfahan-IRAN. Renew Sustain Energy Rev 2017;68(2):986–96. https://doi.org/10.1016/j.rser.2015.07.014.
[60] Izmir development agency (İZKA). Izmir Solar Energy Sector 2016. https://www.kalkinmakukutuphanelesi.gov.tr/assets/upload/dosyalar/zmirde-gunes-enerjisi-sektorunde-yatirim.pdf [accessed 30 Jun 2025].
[61] Izmir Development Agency (İZKA). Wind Energy Sector and Offshore Wind Energy Roadmap for Izmir. Jul 2021, https://izka.org.tr/wp-content/uploads/2021/08/ruzgar_enerjisi_sekto%CC%88ru%CC%88-Izmir_denizustu_ruzgar_enerjisi_yol-haritasi-2.pdf (accessed 08 Aug 2025).
[62] Dehra H. An investigation on energy performance assessment of a photovoltaic solar wall under buoyancy-induced and fan-assisted ventilation system. Appl Energy 2017;191:55–74.
[63] Shang Y, Li Z, Mao R, Wang C. Effects of hillside slopes on the flow field of wind farms. In: 2023 7th International Conference on Smart Grid and Smart Cities (ICSGSC). 2023. https://doi.org/10.1109/ICSGSC59580.2023.10319141. 512–516.
[64] Mondol JD, Yohanis YG, Norton B. The impact of array inclination and orientation on the performance of a grid-connected photovoltaic system. Renew Energy 2007;32(1):118–40. https://doi.org/10.1016/j.renene.2006.05.006.
[65] Pauli H, Efe R, Rehman K, Hakeem I, Faridah-Hanum I, Öztürk M. Climate change impacts on high-altitude ecosystems. Mountain Research and Development 2016;36(1):25–35.

[66] Saaty TL. A scaling method for priorities in hierarchical structures. J Math Psychol 1977;15:234–81. https://doi.org/10.1016/0022-2496(77)90033-5.
[67] Bozóki S, Fülöp J. Efficient weight vectors from pairwise comparison matrices. Eur J Oper Res 2018;264:419–27.
[68] Diakoulaki D, Mavrotas G, Papayannakis L. Determining objective weights in multiple criteria problems: the CRITIC method. Computers & Operations Research 1995;22(7):763–70. https://doi.org/10.1016/0305-0548(94)00059-H.
[69] Malczewski J. GIS and multicriteria decision analysis. John Wiley & Sons. 1999.
[70] Hani HM, Nassar MMNE, Kallali H, El-Din MMN. Sensitivity analysis for multi-criteria decision analysis framework for site selection of aquifer recharge with reclaimed water. Sustainability 2023;15(6):5399. https://doi.org/10.3390/su15065399.
[71] Triantaphyllou E. A sensitivity analysis approach for MCDM methods. In: Multi-criteria decision making methods: A comparative study. Springer; 2000. https://doi.org/10.1007/978-1-4757-3157-6_8.
[72] Feizizadeh B, Jankowski P, Blaschke T. A GIS-based spatially explicit sensitivity and uncertainty analysis approach for multi-criteria decision analysis. Comput Geosci 2014;64:81–95. https://doi.org/10.1016/j.cageo.2013.11.009.
[73] Campello RJGB, Moulavi D, Sander J. Density-based clustering based on hierarchical density estimates (HDBSCAN). In: Advances in Knowledge Discovery and Data Mining (PAKDD) 2013. https://doi.org/10.1007/978-3-642-37456-2_14.
[74] Moreira A, Santos MY. Concave hull: a k-nearest neighbours approach for the computation of the region occupied by a set of points. In: Proceedings of GRAPP 2007:61–8.
[75] Hwang CL, Yoon K. Multiple attribute decision making: methods and applications—a state-of-the-art survey. Springer; 1981. https://doi.org/10.1007/978-3-642-48318-9.
[76] Asaeedi S, Didehvar F, Mohades A. α-Concave hull, a generalization of convex hull. Theor Comput Sci 2017;702:48–59. https://doi.org/10.1016/j.tcs.2017.08.014.
[77] Pamučar D, Ćirović G, Božanić D. Application of the multi-attributive border approximation area comparison (MABAC) method for decision making in road traffic safety. Decision Science Letters 2015;4(3):367–80. https://doi.org/10.1016/j.eswa.2014.11.057.
[78] Breiman L. Random forests. Mach Learn 2001;45:5–32. https://doi.org/10.1023/A:1010933404324.
[79] Rousseeuw PJ. Silhouettes: a graphical aid to the interpretation and validation of cluster analysis. J Comput Appl Math 1987;20:53–65. https://doi.org/10.1016/0377-0427(87)90125-7.
[80] Caliński T, Harabasz J. A dendrite method for cluster analysis. Commun Stat 1974;3(1):1–27. https://doi.org/10.1080/03610927408827101.
[81] Davies DL, Bouldin DW. A cluster separation measure. IEEE Trans Pattern Anal Mach Intell 1979;1(2):224–7. https://doi.org/10.1109/TPAMI.1979.4766909.